

Bulking Up the Bay-Position Substituents Enables Enhanced Selectivity of C_s -Symmetric Boron Subphthalocyanine–Subnaphthalocyanine Hybrids

Nina F. Farac, Alan J. Lough, and Timothy P. Bender*



Cite This: *Precis. Chem.* 2024, 2, 161–181



Read Online

ACCESS |

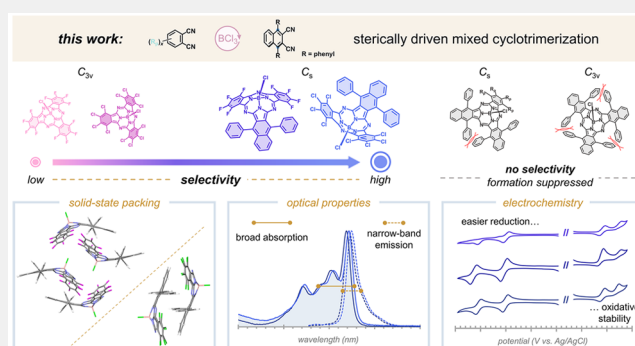
Metrics & More

Article Recommendations

Supporting Information

ABSTRACT: The precise synthesis of subporphyrinoid hybrids with π -expanded topologies and unique material properties plays a promising role in the design of functional macrocycles. Easy, selective, and controllable routes to boron subphthalocyanine–subnaphthalocyanine hybrids, Bsub(Pc_{3-p} - Nc_p)_s, are desirable for this purpose yet synthetically challenging due to random mixtures of C_s -, C_{3v} -, and, in some cases, C_1 -symmetric compounds that form during traditional statistical mixed cyclotrimerizations. Herein, we addressed this issue by developing a sterically driven mixed cyclotrimerization with enhanced selectivity for the targeted C_s -symmetric hybrid and complete suppression of sterically crowded macrocyclic byproducts. This process, coupled with a rationally designed precursor bearing bulky phenyl substituents, enabled the synthesis and characterization of bay-position phenylated Ph_2 -(R_p)₈Bsub(Pc_2 - Nc_1) hybrids with halogens (R_p = Cl or F) in their peripheral isoindole rings. Reaction selectivity ranged between 59 and 72% with remarkable yields, significantly higher than that of conventional mixed cyclotrimerizations. These findings were augmented by theoretical calculations on precursor Lewis basicity as guiding principles into hybrid macrocycle formation. Additionally, the incorporation of unfused phenyl groups and halogen atoms into the hybrid framework resulted in fine-tuned optical, structural, electronic, and electrochemical properties. This straightforward approach achieved improved selectivity and controlled narrowing of the product distribution, affording the efficient synthesis of structurally sophisticated Bsub(Pc_2 - Nc_1) hybrids. This then expands the library of 3-dimensional π -extended macrocycles for use in a range of applications, such as in optoelectronic devices with precisely tailored optical properties.

KEYWORDS: subphthalocyanine, hybrids, low-symmetry aromatic macrocycle, selective cyclotrimerization, sterically driven chemistry, broad absorption, material properties



1. INTRODUCTION

As the name suggests, boron subphthalocyanine–subnaphthalocyanine hybrids are structural combinations of a boron(III) subphthalocyanine (BsubPc, **Figure 1a**) and boron(III) subnaphthalocyanine (BsubNc, **Figure 1c**). BsubPcs have garnered considerable attention as functional materials in organic electronics due to their intriguing 14π -aromatic systems and bowl-shaped curved structures.^{1,2} BsubPcs are boron-complexed, ring-contracted porphyrinoids comprised of three aza-bridged 1,3-diiminoisoindole units as the scaffold and a substituent extending perpendicularly from the boron center, known as the axial position. BsubNcs display the same nonplanar molecular geometry and C_{3v} symmetry as BsubPcs but differ by an elongated π -conjugation system composed of three 1,3-diiminobenz(*f*)-isoindoline units. Outcomes of the longer π -conjugated system include narrower HOMO–LUMO band gaps and heavily red-shifted absorption and fluorescence spectra (i.e., 630–680 nm) compared to those of BsubPcs (i.e., 550–600 nm), which justify the growing interest in BsubNcs as

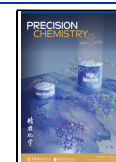
chromophores for capturing red photons in organic solar cells (OSCs).^{3–7} Another notable distinction is that the composition of axially chlorinated boron subnaphthalocyanine (i.e., Cl-BsubNc), whether synthesized from literature methods or supplied commercially, is a mixed alloyed composition of derivatives that are randomly chlorinated in the bay positions (**Figure 1c**).⁸ Our lab identified this alloyed mixture as chloro-(chloro)_{*n*}-boron subnaphthalocyanines (Cl-Cl_{*n*}BsubNcs, where *n* = is the number of bay-position chlorines ranging between 0 and 6) and studies have demonstrated that this random bay-position chlorination positively impacts OSC performance.^{5,8} A

Received: February 5, 2024

Revised: March 18, 2024

Accepted: March 20, 2024

Published: April 4, 2024



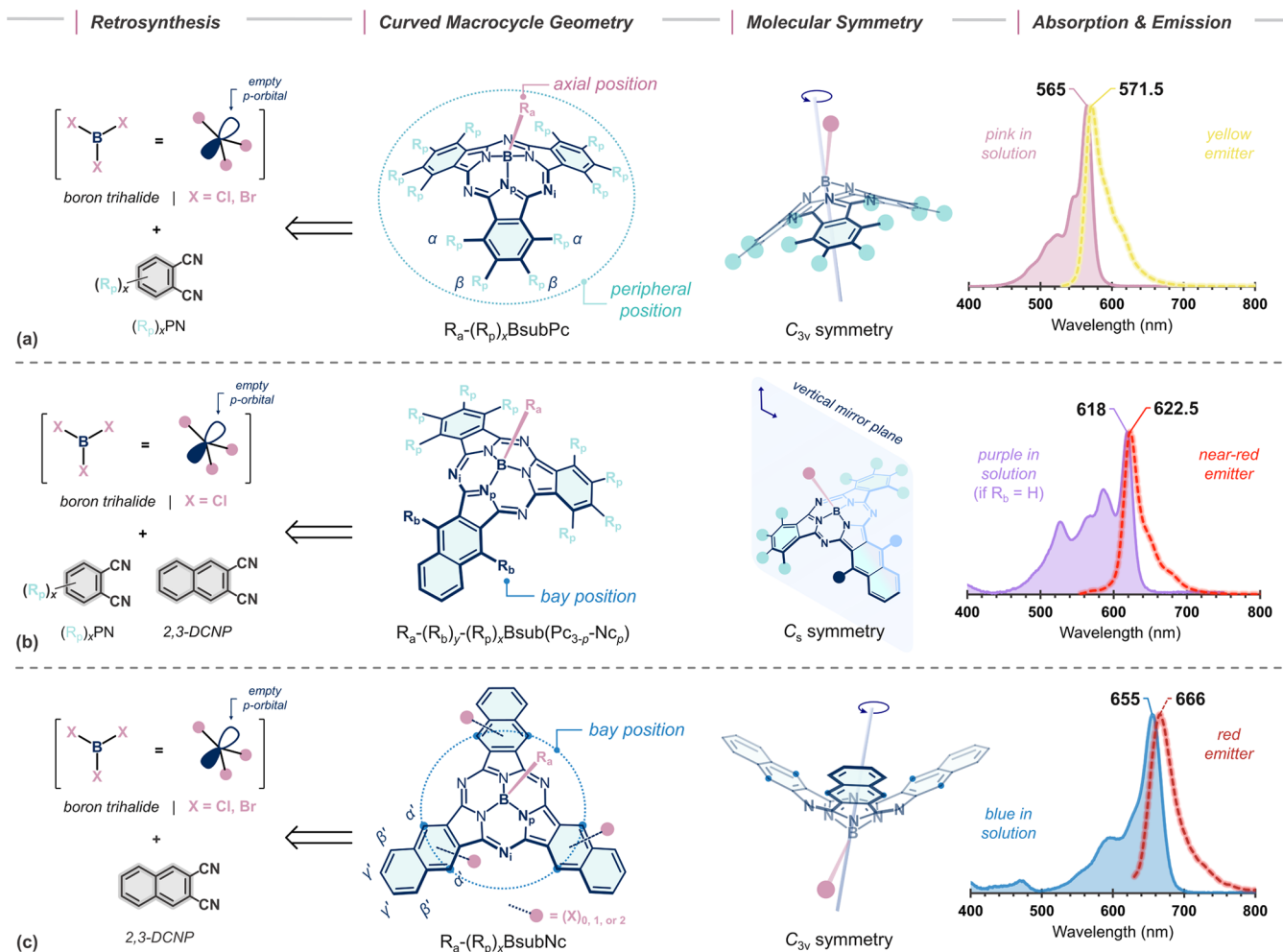


Figure 1. Retrosynthesis, general nonplanar geometry, molecular symmetry, and normalized solution-state absorption and fluorescence spectra of (a) boron subphthalocyanine (BsubPc), (b) boron subphthalocyanine–subnaphthalocyanine hybrid [Bsub(PC_{3-p}-Nc_p)], and (c) boron subnaphthalocyanine (BsubNc). General molecular structures include the following designations: R_a is an axial position moiety, R_b is a bay-position substituent, R_p is a peripheral position substituent, N_p is a pyrrole nitrogen, N_i is an imine nitrogen, α and β are the “alpha” and “beta” positions on the BsubPc isoindole units, respectively, and α', β', and γ' are substituent labels on the benz(f) isoindole units of BsubNcs and Bsub(PC_{3-p}-Nc_p) hybrids. The solution-state spectral data of Cl-BsubPc, Cl-F₈Bsub(PC₂-Nc₁) (x = 8, p = 1), and Cl-Cl_nBsubNc were acquired in toluene at room temperature.

breakthrough device efficiency of 8.4% by pairing the complementary absorption of Cl-BsubNc to that of Cl-BsubPc³ set the stage for further investigations into the functionality of these molecules in other OSC device architectures.^{7,9–11}

Other remarkable features of BsubPcs and BsubNcs include narrow fluorescence profiles,¹² high ambient stability,^{13,14} and tunable material properties via chemical functionalization of the axial and/or peripheral positions.^{15–17} Both macrocycles have a well-established synthesis methodology by templated cyclotrimerization of an *ortho*-dinitrile (e.g., phthalonitriles for BsubPcs; 2,3-dicyanonaphthalene or a derivative of it for BsubNcs) with a trivalent boron Lewis acid (e.g., boron trichloride, BCl₃, or boron tribromide, BBr₃) in an aromatic solvent. In the context of BsubPc and BsubNc chemistry, cyclotrimerization refers to the trimerization of three *o*-dinitrile units to form a cyclic, aromatic macrocycle in the presence of a trivalent boron Lewis acid (Figure 1, retrosynthesis). This templated cyclotrimerization also encompasses mixed cyclotrimerization (also referred to as statistical cross-condensation or cocyclization) of two different *o*-dinitrile precursors to access new diiminoisoindole-hybridized analogues with fundamentally

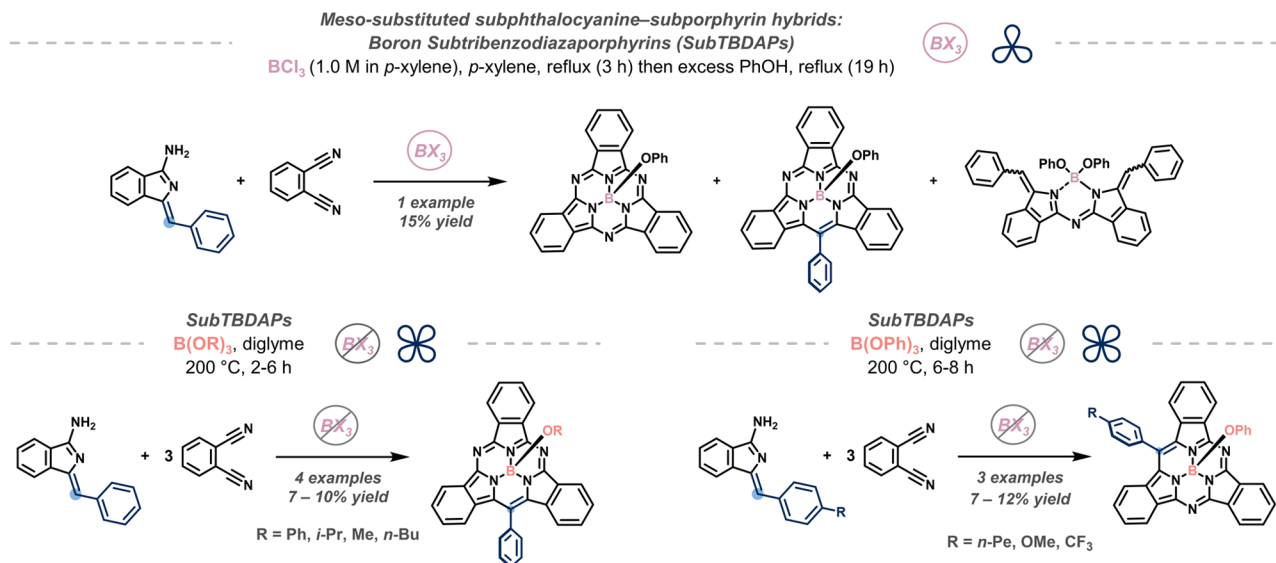
different physicochemical properties. Mixed cyclotrimerization typically forms hybrid BsubPc macrocycles with lower molecular symmetry (e.g., C_s symmetry) and altered spectroscopic properties.^{4,18–30} This approach has been further applied for the preparation of π-extended BsubPc hybrids with two-oxygen-bridged aromatic fragments,³¹ pyrene-fused diiminoisoindole units,³² core-expanded inner pyrrolic rings,^{33–35} and benzo-annulated units.^{36–40}

From this category, BsubPc–BsubNc hybrids (broadly abbreviated as Bsub(PC_{3-p}-Nc_p) hybrids; Figure 1b) are low-symmetry macrocycles that blend the molecular structures of BsubPcs and BsubNcs into one material possessing uniquely intermediate properties and their synthesis was first reported by Stork et al. in 1999.³⁹ By reacting 3,4,5,6-tetrafluorophthalonitrile (TFPN) and 2,3-dicyanonaphthalene (2,3-DCNP) with BCl₃, a series of partially fluorinated and benzo-annulated BsubPc–BsubNc hybrids were prepared that we have previously denoted as R_a-F_xBsub(PC_{3-p}-Nc_p)s. We recently studied and found that R_a-F_xBsub(PC_{3-p}-Nc_p) hybrids, where R_a = axial chloride (Cl–) or axial fluoride (F–), x = 8, and p = 1, exhibit broad absorption with red-shifted Q bands, narrow near-red

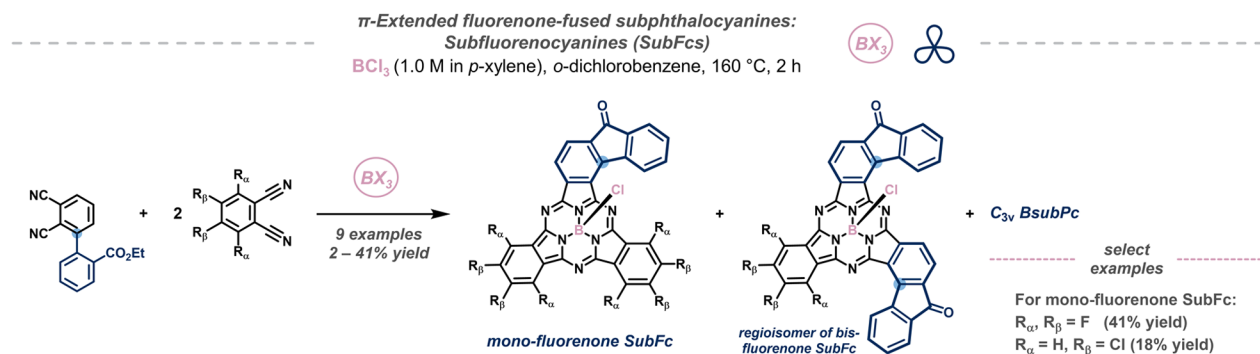
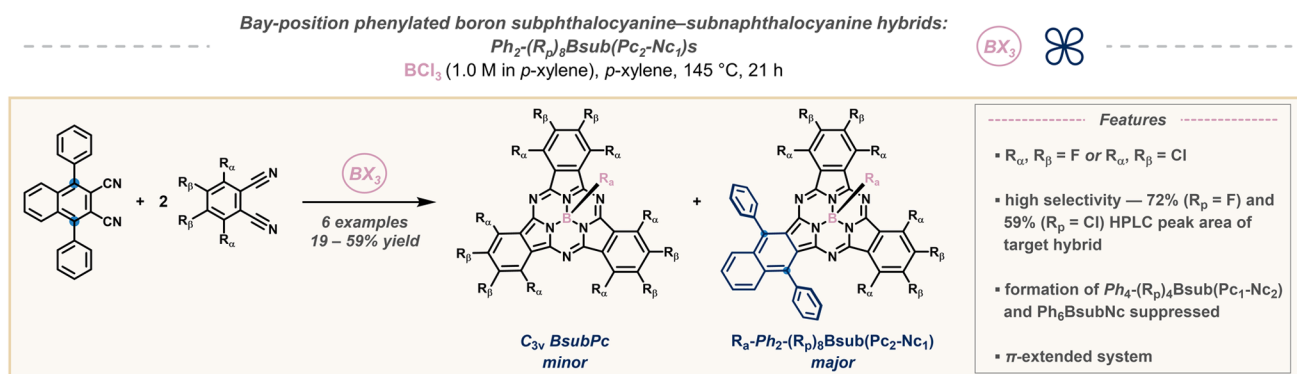
Scheme 1. Recent Strategies for Hybrid Synthesis of Low-Symmetry Boron(III) Subphthalocyanines and Subporphyrinoids in the Context of This Work



A | Cross-condensation between phthalonitrile and non-nitrile components (Camidge, 2015)



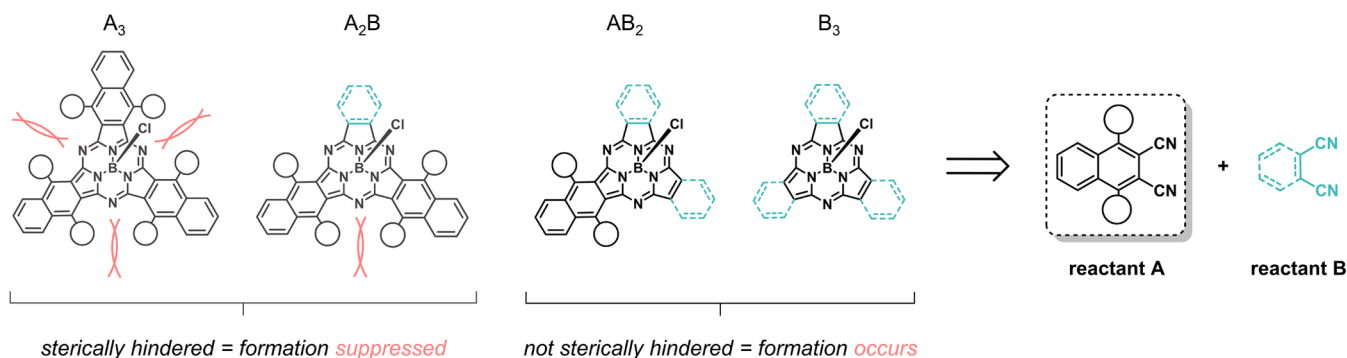
B | Cross-cyclotrimerization of phthalonitriles with intramolecular Friedel–Crafts acylation (Torres, 2019)

C | Sterically driven mixed cyclotrimerization between two different *o*-dinitriles (this work)

emission, high molar absorptivity, and dual electrochemical reversibility.³⁶ Our study also highlighted a major synthetic drawback of mixed cyclotrimerization, mainly the formation of a statistical mixture of randomly distributed products which varied in the number and position of ring substituents. The products

were separated using standard chromatographic techniques, though solubility issues and/or intermolecular interactions between different derivatives posed challenges. Steric factors and the relative reactivities of *o*-dinitriles toward the boron reagent may influence the selectivity of mixed cyclotrimeriza-

Scheme 2. Retrosynthesis of Sterically Driven Mixed Cyclotrimerization to Enhance Selectivity of $R_a-(R_p)_x\text{Bsub}(\text{Pc}_{3-p}\text{-Nc}_p)$ Hybrids, Where $x = 8$ and $p = 1$



tion, though a clear tendency has yet to be determined due to the scarcity of studies on this topic.⁴¹ In general, the selectivity of mixed cyclotrimerization reactions can be partially controlled by tuning the stoichiometric molar ratio between the starting *o*-dinitriles.^{36,41}

Despite partial stoichiometric control of this reaction type to $R_a\text{-F}_x\text{Bsub}(\text{Pc}_{3-p}\text{-Nc}_p)$ hybrids, enhanced selectivity and precise control of the product distribution remain issues to be addressed. The synthetic challenge of the π -extended hybrid structure stems from limited synthesis methods available, and only few studies have been reported to-date.⁴² Nevertheless, elegant contributions toward the controlled formation of π -extended BsubPc-based hybrid systems have been made including templated and one-pot postfunctionalization synthesis.^{43,44} Core-hybridized, meso-substituted BsubPcs, boron(III) subtribenzodiazaporphyrins, were reported by Cammidge et al. using a BCl_3 - or trialkoxyborate-templated synthesis between a preformed aminoisindolene and phthalonitrile (Scheme 1A).⁴³ Another notable example is a series of subphthalocyanine hybrids bearing fluorenone-fused units, boron(III) subfluorenonecyanines (SubFcs), formed by Torres et al. using an innovative one-pot synthesis that consists of the standard mixed cyclotrimerization of phthalonitriles followed by an *in situ*, intramolecular Friedel–Crafts acylation (Scheme 1B).⁴⁴ Despite developments in diversely functionalized hybrid structures, these examples did not emphasize precise control over the product distribution to selectively form target molecules; rather, desired hybrids were isolated from statistical mixtures containing at least three separate chromophores.

Therefore, these limitations prompted us to explore alternative routes for a more controlled and selective preparation of π -extended subporphyrinoid hybrids, particularly BsubPc–BsubNc hybrids as functional macrocycles for organic electronics.

Several synthetic approaches have been developed in the past for the formation of asymmetric phthalocyanines (Pcs) and their analogues, which are formed via cyclotetramerization and are higher homologues of BsubPcs and BsubNcs.⁴⁵ Among these strategies, an interesting modification to the statistical cross-condensation method involves one of the *o*-dinitriles (e.g., reactant A) bearing bulky rigid groups in both α positions (3,6- α,α positions of phthalonitrile derivatives, or 1,4- α,α' positions of 2,3-DCNP derivatives) to preferentially form the less sterically hindered Pc macrocycles.⁴⁵ If we extend this to BsubPc chemistry, the steric hindrance between bulky groups in close vicinity should significantly suppress formation of sterically strained A_3 and A_2B compounds while formation of less

sterically crowded AB_2 and B_3 macrocycles should be favored (Scheme 2). Theoretically, this type of mixed cyclotrimerization should demonstrate improved selectivity producing only two macrocycles that display minimal to no steric hindrance. Therefore, this sterically driven strategy offers a simple yet still elegant route toward selective formation of π -extended Bsub($\text{Pc}_{3-p}\text{-Nc}_p$) hybrids, with potentially higher yields than other sophisticated methods used in phthalocyanine (Pc) chemistry.^{46,47}

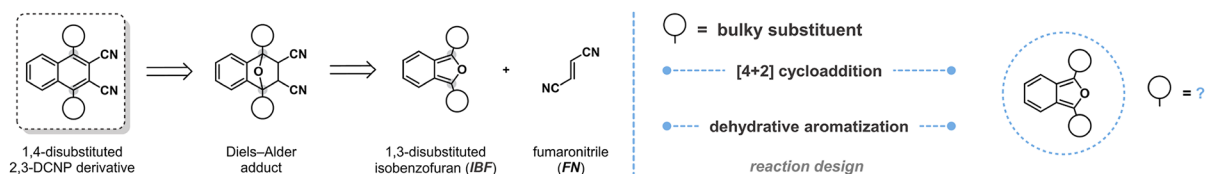
Inspired by these precedents, we report the use of sterically driven mixed cyclotrimerization enabling precise control over the product distribution to two macrocyclic species for the selective formation of Bsub($\text{Pc}_2\text{-Nc}_1$) hybrids (Scheme 1C). The primary macrocycle from this process was the targeted nonsterically hindered C_2 -symmetric hybrid. This resulted in a series of new, π -extended BsubPc–BsubNcs termed $R_a-(R_b)_y-(R_p)_x\text{Bsub}(\text{Pc}_{3-p}\text{-Nc}_p)$ hybrids where R_a is the axial substituent (Cl–, F–, or PhO–), R_b represents the bay-position phenyl groups ($R_b = \text{Ph}$), R_p denotes the peripheral halogens (Cl– or F–), $y = 2$, $x = 8$, and $p = 1$. This approach involved a rationally designed dicyanonaphthalene-based precursor with phenyl groups in the α' positions to establish steric hindrance, while BCl_3 simultaneously acts as the template and Lewis acid catalyst. The achieved purities, yields, and selectivity (59% when $R_p = \text{Cl}$ and 72% when $R_p = \text{F}$) in this work far surpass those in comparable mixed cyclotrimerizations, outperforming cases involving flexible α' -positioned thiophenol groups⁴⁸ or fused fluorenone moieties.⁴⁴ This highlights the importance of structural rigidity and geometric orientation of the sterically bulky substituent in determining the precision of this approach. Notably, our method achieves multifaceted success, delivering high selectivity, controlled synthesis, and simultaneous suppression of sterically crowded macrocyclic byproducts and random bay-position halogenation. Furthermore, characterization of the new $R_a\text{-Ph}_2\text{-(R}_p)_8\text{Bsub}(\text{Pc}_2\text{-Nc}_1)$ chromophores unraveled the impact of bay-position phenyl group introduction on their structural, optical, electronic, and electrochemical properties. This work demonstrated the excellent potential of the sterically driven mixed cyclotrimerization approach for synthetic control of π -extended, low-symmetry hybrid macrocycles as promising optoelectronic materials.

2. RESULTS AND DISCUSSION

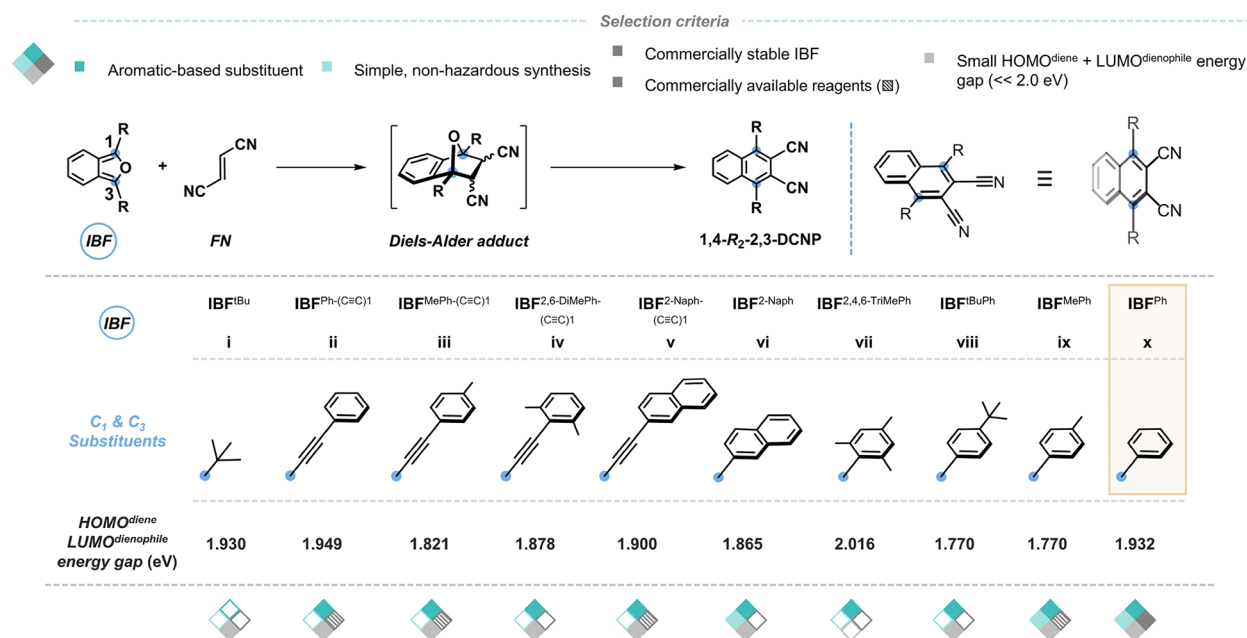
2.1. Design and Synthesis of the Sterically Hindered Precursor

To improve selectivity of Bsub($\text{Pc}_{3-p}\text{-Nc}_p$) hybrid formation, we leveraged steric hindrance by selecting a bulky rigid substituent

A | Retrosynthetic template for precursor design considered in this work



B | DFT calculations of various isobenzofurans for Diels-Alder stereoelectronics



C | Formation of Diels-Alder adduct: HOMO-LUMO Energy Level Matching

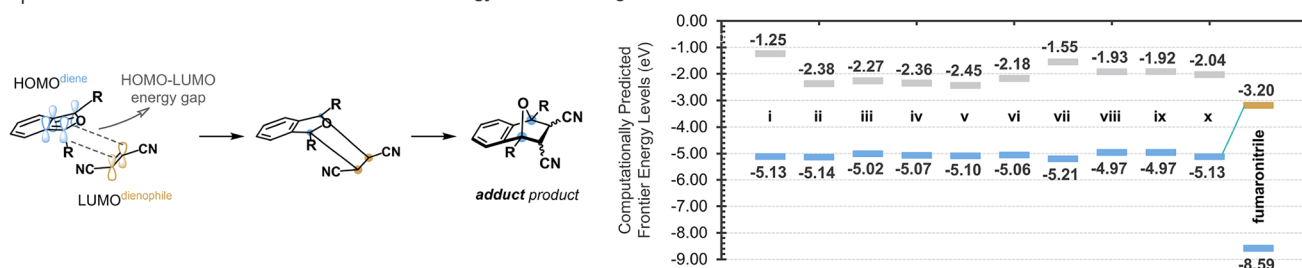


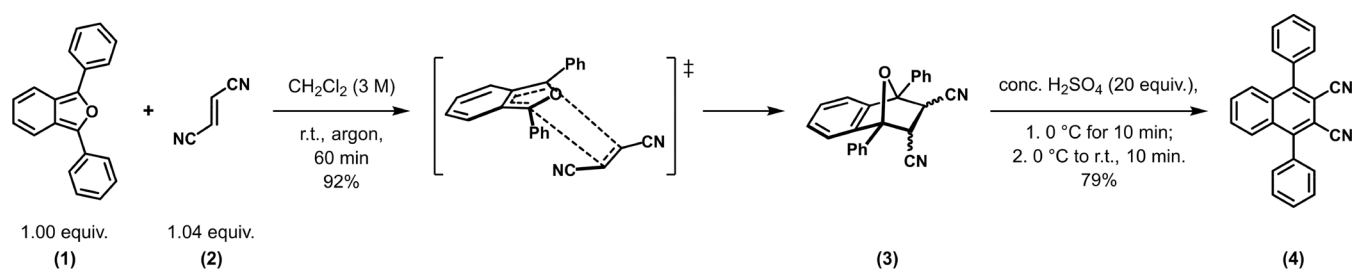
Figure 2. Design and optimization of the 1,4-disubstituted 2,3-dicyanophthalene precursor. (A) Retrosynthetic blueprint consisting of a Diels-Alder [4 + 2] cycloaddition and dehydrative aromatization starting from a 1,3-disubstituted isobenzofuran and fumaronitrile. (B) Template reaction with precursor design criteria, bulky substituent candidates, and Diels-Alder stereoelectronic considerations. Teal and gray squares represent different design criteria, with filled squares indicating satisfied criteria and unfilled squares denoting unmet criteria. HOMO^{diene}–LUMO^{dienophile} energy gaps calculated using the B3LYP/6-311G level. (C) Computationally predicted HOMO/LUMO energy levels for isobenzofurans i–x and fumaronitrile for the formation of Diels-Alder adducts.

for the 1,4- α' , α' positions of 2,3-DCNP. Opting to functionalize 2,3-DCNP over phthalonitrile served the dual purpose of blocking the 1,4- α' , α' positions, preventing random bay-position halogenation,⁸ and further narrowing the product distribution by eliminating randomly halogenated byproducts.

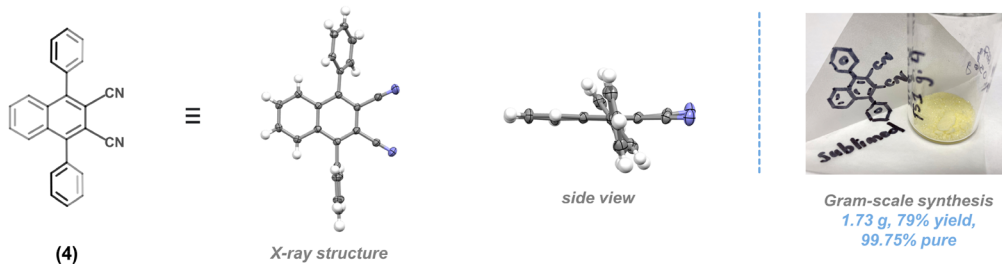
To procure 1,4-disubstituted 2,3-DCNP derivatives, we aimed for a simple synthetic blueprint consisting of a Diels-Alder [4 + 2] cycloaddition between the respective 1,3-disubstituted isobenzofuran (IBF) and fumaronitrile followed by a dehydrative aromatization (Figure 2A). We also considered the stereoelectronics of Diels-Alder type reactions via DFT calculations. Specifically, some 1,3-disubstituted IBFs can react more favorably with fumaronitrile given there is a small

HOMO–LUMO energy gap between the diene and dienophile (Figure 2B,C). We screened different 1,3-disubstituted IBFs using four main design criteria to refine our selection (Figure 2B, criteria represented by teal and gray squares): (1.) the substituents in the 1,3-positions should be aromatic-based as additional π -conjugation is generally beneficial for organic electronics; (2.) the 1,3-disubstituted IBF is ideally commercially stable or if it cannot be sourced from a supplier, then (3.) the isobenzofuran can be produced from a simple, non-multistep, non-hazardous synthesis using commercially stable starting reagents; and (4.) the HOMO–LUMO energy gap between the 1,3-disubstituted IBF and fumaronitrile is small (i.e., $\ll 2.0$ eV). We computed 20 isobenzofurans using B3LYP/

Scheme 3. Synthetic Route, Scale-Up, and Single-Crystal X-ray Characterization of 1,4-*Ph*₂-2,3-DCNP (4) in the Context of This Work^a



Scale-up synthesis & X-ray characterization of 1,4-*Ph*₂-2,3-DCNP



^aConditions for gram-scale synthesis: 1,3-diphenylisobenzofuran (1) (2.01 g, 7.42 mmol, 1.0 equiv) and fumaronitrile (2) (0.602 g, 7.71 mmol, 1.04 equiv) in dichloromethane (5.25 mL, 3.0 M) at room temperature under argon for 60 min to isolate Diels–Alder adduct (3). Then adduct (3) (2.318 g, 6.65 mmol, 1.0 equiv) was stirred in sulfuric acid (7.12 mL, 132.8 mmol, 20 equiv) at 0 °C for 10 min, and then stirred and warmed up to room temperature for 10 min.

6-311G level of theory and more specifically defined the range to 10 possible options as outlined in Figure 2B. All isobenzofurans except for IBF vii displayed a small HOMO^{diene}–LUMO^{dienophile} energy gap with respect to fumaronitrile. However, IBFs ii, iii, and v are not commercially stable nor readily supplied, and their syntheses consist of a multistep protocol including double nucleophilic additions of alkynyllithiums to *o*-phthalaldehyde and manganese-catalyzed selective oxidation.⁴⁹ On the other hand, Benderradij et al.⁵⁰ developed a convenient single-step synthesis for the formation of IBFs vi and ix using aryl Grignard reagents, but the starting reagent required for this process (i.e., 3-methoxy-3*H*-isobenzofuran-1-one) is costly. Out of these 10 DFT-computed compounds, IBF x (i.e., 1,3-diphenylisobenzofuran) met all four design criteria including being commercially stable and readily available from suppliers. The HOMO–LUMO energy gap between isobenzofuran x and fumaronitrile was calculated to be 1.932 eV which is adequately small (Figure 2C). In result, we chose phenyl (Ph) groups as our bulky rigid substituent.

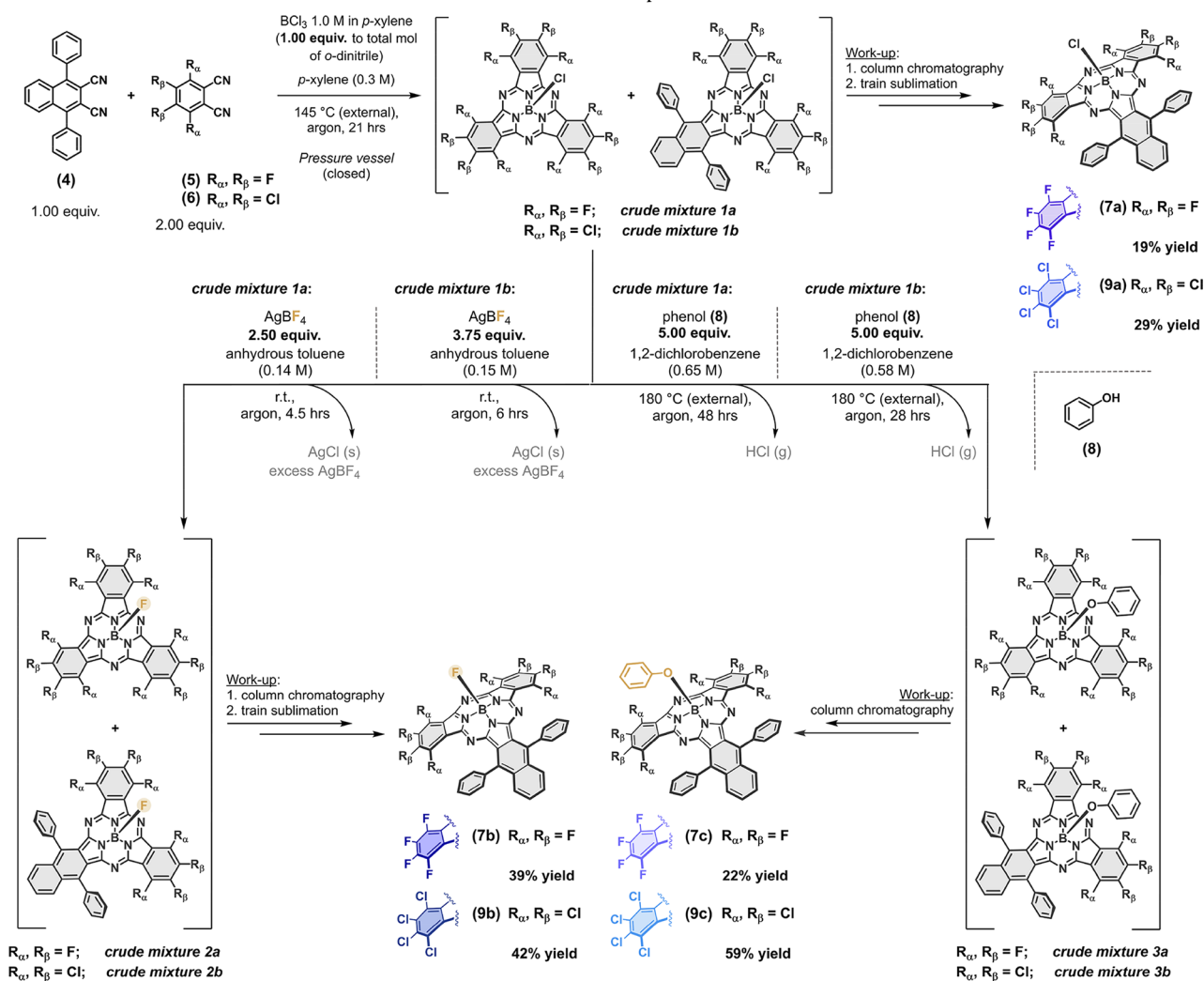
To produce the bay-position phenylated 2,3-DCNP derivative, we modified a literature procedure reported by de Souza et al.⁵¹ in which 1,3-diphenylisobenzofuran (1) reacts with fumaronitrile (2) via a Diels–Alder [4 + 2] cycloaddition to produce Diels–Alder adduct (3). The isolated adduct (3) was then smoothly converted to 1,4-diphenyl-2,3-dicyanonaphthalene (4) (also denoted as 1,4-*Ph*₂-2,3-DCNP) by subsequent acid-promoted cyclization (Scheme 3). Modifications to the literature procedure included a non-stepwise addition of (2), using 20 equiv of sulfuric acid ($\times 1.5$ the original amount) to ensure full conversion from adduct (3) to (4), replacing column chromatography with train sublimation as the ultimate purification technique, and increasing the process to the gram scale (Scheme 3). Single crystals of 1,4-*Ph*₂-2,3-DCNP (4) obtained from the slow evaporation of chloroform (CCDC 2305675) or acetone (CCDC 2305676) highlight that, in the

solid state, the steric hindrance arises from the phenyl groups being oriented almost perpendicular to the naphthalene core (Scheme 3).

2.2. Optimization of Sterically Driven Mixed Cyclotrimerization to Cl-*Ph*₂-F₈Bsub(PC₂-Nc₁) Hybrid

We initially attempted the mixed cyclotrimerization of 1,4-*Ph*₂-2,3-DCNP (4) with the highly reactive 3,4,5,6-tetrafluorophthalonitrile (TFPN, (5)) under the conditions of Method 5.6 and Method 5.7 reported in our recent work on F₈Bsub(PC₂-Nc₁) hybrids.³⁶ This resulted in recovering most of the starting material (4) with no conversion to the desired hybrid, thus suggesting a substantial lack of reactivity under these earlier reported conditions. In contrast, the cross-cyclotrimerization between (4) and (5) templated by BCl₃ (1.0 M in *p*-xylene) in *p*-xylene solvent and carried out within a sealed, heavy-walled pressure vessel led to the selective formation of Cl-*Ph*₂-F₈Bsub(PC₂-Nc₁) (7a) in 19% yield (Scheme 4). The only other significantly produced macrocyclic species in this mixture was the C_{3v} symmetric perfluorinated BsubPc, Cl-F₁₂BsubPc. The sterically crowded species, Cl-*Ph*₄-F₄Bsub(PC₁-Nc₂) (where $y = 4$, $x = 4$, and $p = 2$) and Cl-Ph₆BsubNc, could not be detected either by HPLC or DART high resolution mass spectrometry (DART-HRMS [M + H]⁺) of the reaction crude and were therefore not formed (Figures S8, S9, S42). In this case, the higher pressure brought on by a closed atmosphere significantly enhanced the reactivity of (4), giving rise to more reactive intermediates which primarily evolved toward the formation of the highly soluble hybrid (7a).

The variation in reaction conditions (i.e., temperature, *o*-dinitrile stoichiometric ratio, and time) allowed for optimization to selectively obtain (7a) in good yield within BsubPc chemistry. The highest selectivity for (7a) (average HPLC MaxPlot peak area of 72%) was obtained upon heating a 1:2 stoichiometric ratio of (4) and (5) in the presence of BCl₃ (1.0 M in *p*-xylene)

Scheme 4. Synthetic Routes for Bay-Position Phenylated R_{α} - Ph_2 -(R_{β}) $_8$ Bsub(Pc_2 - Nc_1) Hybrids in the Context of This WorkTable 1. Optimization of Synthetic Conditions for Maximizing Selectivity in the Formation of Bay-Position Phenylated Hybrid Cl - Ph_2 - F_8 Bsub(Pc_2 - Nc_1) (7a)^a

entry ^b	molar ratio (1,4- Ph_2 -2,3-DCNP:TFPN)	BCl_3 solvent (equiv BCl_3)	reaction concentration (M)	external reaction temperature (°C)	time (h)	crude yield	number of macrocycles in mixture; peak area of Cl - Ph_2 - F_8 Bsub(Pc_2 - Nc_1) (7a) ^c
1	(1:1)	1.0 M in <i>p</i> -xylene (1.00 equiv)	0.3	145	20	>100%	6; 42%
2	(1:1)	1.0 M in <i>p</i> -xylene (1.00 equiv)	0.3	165	20	>100%	5; 33%
3	(1:2)	1.0 M in <i>p</i> -xylene (1.00 equiv)	0.3	145	20	>100%	3; 69%
4 ^d	(1:2)	1.0 M in <i>p</i> -xylene (1.00 equiv)	0.3	145	21	>100%	2; 72%
5	(1:2)	1.0 M in <i>p</i> -xylene (1.00 equiv)	0.3	145	22	>100%	4; 48%

^a1,4- Ph_2 -2,3-DCNP = 1,4-diphenyl-2,3-dicyanonaphthalene (4); TFPN = 3,4,5,6-tetrafluorophthalonitrile (5); BCl_3 = boron trichloride. ^bAll runs were carried out in a sealed, heavy-walled pressure vessel. ^cThe number of macrocycles was determined from HPLC plots (500–800 nm channel) with a threshold peak area of >1.00% to be considered a significant macrocyclic constituent in the mixture. The peak area for (7a) was assessed using HPLC MaxPlots. ^dProcess was replicated four times with HPLC MaxPlot peak areas ranging between 69.08–74.44% for (7a), with an average MaxPlot peak area of 72.25%.

in *p*-xylene at 145 °C for 21 h (Entry 4, Table 1). Under these conditions, C_{3v} -symmetrical Cl - F_{12} BsubPc was obtained with HPLC MaxPlot peak areas <20%, and a chlorinated byproduct of (7a), presumably formed via electrophilic aromatic substitution, showed a MaxPlot peak area of <1%. The reaction

temperature for Entry 4 (Table 1) was maintained slightly above the boiling point of *p*-xylene at 145 °C, consistent with our previous work.³⁶ Other attempts at increasing selectivity revealed that reaction time is an important factor in the synthesis of (7a). Extending the reaction to 22 h (Entry 5, Table

HPLC Chromatograms of Mixed Cyclotrimerizations with 1,4-*Ph*₂-2,3-DCNP compared to 2,3-DCNP

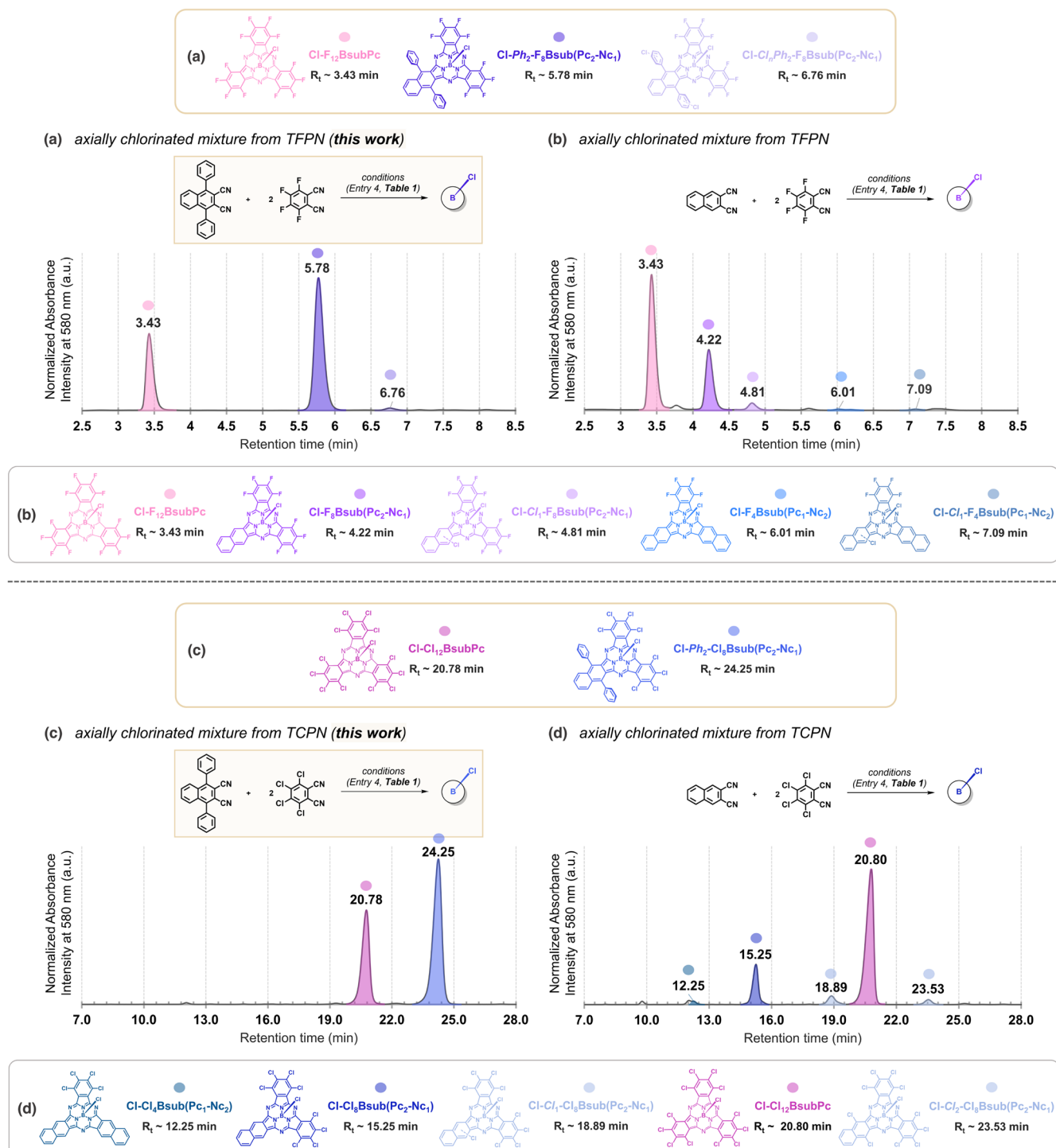


Figure 3. HPLC chromatograms (580 nm channel) of axially chlorinated, crude Bsub(PC_{3,p}-Nc_p) hybrid mixtures produced from the mixed cyclotrimerization of (a) 1,4-*Ph*₂-2,3-DCNP:TFPN, (b) 2,3-DCNP:TFPN, (c) 1,4-*Ph*₂-2,3-DCNP:TCPN, and (d) 2,3-DCNP:TCPN. All reactions were carried out using the optimal conditions (Entry 4, Table 1): *o*-dinitrile stoichiometric ratio of (1:2), 1.00 equiv of BCl₃ (1.0 M in *p*-xylene) to the total mol of *o*-dinitrile, *p*-xylene solvent (0.3 M), external reaction temperature of 145 °C, and run for 21 h in a sealed, heavy-walled pressure vessel. Each hybrid chromophore that was identified by DART-HRMS [M + H]⁺ is labeled with their respective HPLC retention time.

1) decreased selectivity for hybrid (7a) and increased the number of macrocycles in the crude mixture.

Interestingly, under the same optimal conditions listed in Entry 4 (Table 1), the mixed cyclotrimerization of 2,3-DCNP and (5) resulted in drastically reduced selectivity for the

F₈Bsub(PC₂-Nc₁) hybrid. The predominant macrocycle within the statistical distribution became the C_{3v}-symmetric Cl-F₁₂BsubPc (Figure 3a vs 3b). This emphasizes the crucial role of introducing phenyl groups in the 1,4- α,α' positions of 2,3-DCNP for enhancement in Bsub(PC₂-Nc₁) selectivity in the

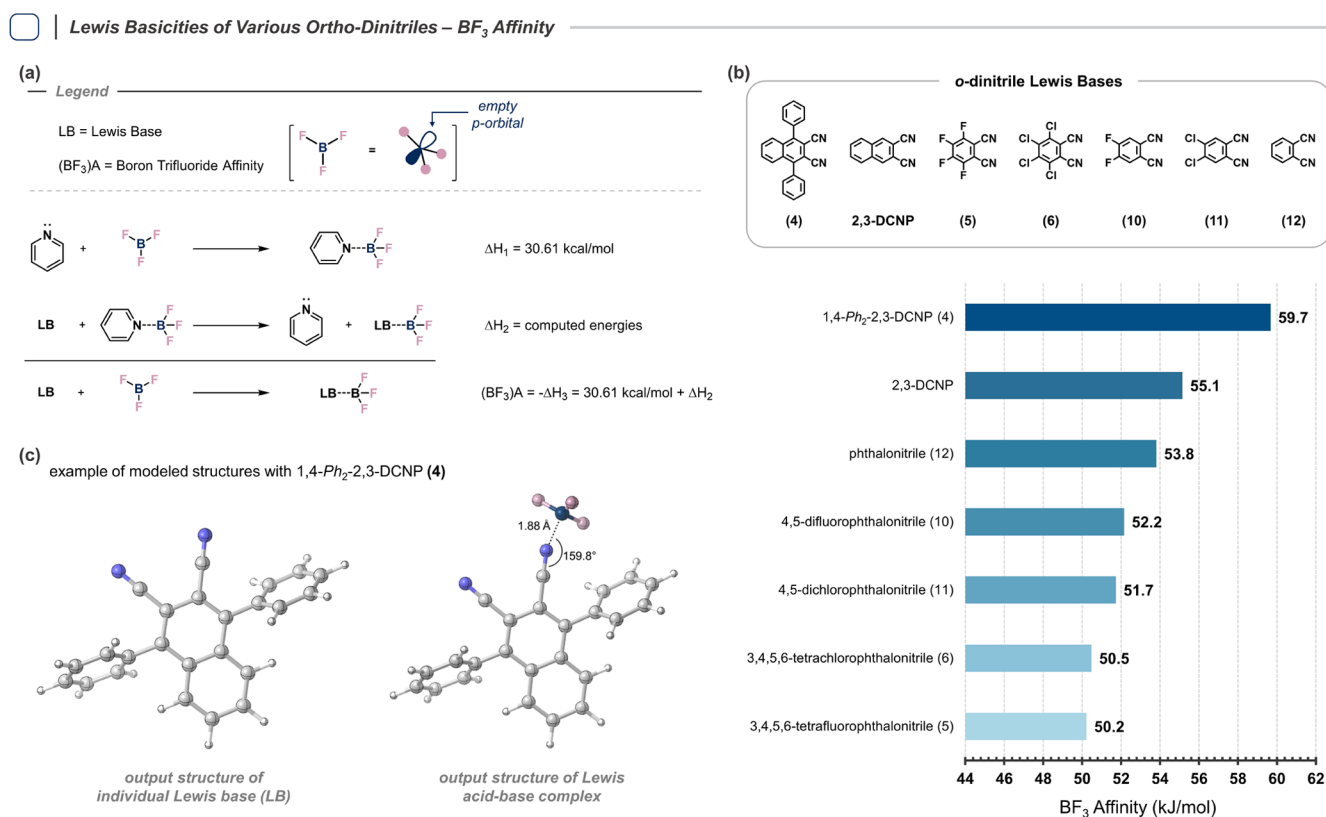


Figure 4. (a) BF₃ affinity method for computing the Lewis basicity⁶³ of precursor *o*-dinitriles where LB is the Lewis base of interest, (BF₃)A is the calculated boron trifluoride affinity, and pyridine is the reference Lewis base. (b) Computed BF₃ affinities of the *o*-dinitrile precursors investigated in this study and of 2,3-dicyanonaphthalene. Calculations were executed using the B3LYP/6-31G(d) level of theory. (c) Modeled structures of the individual Lewis base and the Lewis acid–base complex using 1,4-*Ph*₂-2,3-DCNP (4) as an example *o*-dinitrile. CYLview⁶⁴ was used to visualize input and output structures.

sterically driven mixed cyclotrimerization developed here. Therefore, an appropriate pathway for achieving higher yields of Bsub(Pc₂-Nc₁) hybrids has been demonstrated.

2.3. Stabilizing the Axial Boron–R_a Bond

The higher reactivity of the axial B–Cl bond compared to the axial B–F and B–O bonds has been demonstrated, with the order of thermodynamic stability being B–F > B–O > B–Cl.^{52,53} Additionally, the axial B–Cl bond exhibits liability to ligand exchange in the presence of nucleophiles in solution^{52,54} and is prone to hydrolysis under certain conditions,⁵³ highlighting its greater susceptibility to substitution compared to the B–F and B–O bonds. Seeking stronger and more stable bonds, we synthesized axially fluorinated and axially phenoxyated derivatives with B–F and B–O bonds, respectively. The mechanism for axial exchange from a B–Cl to a B–F bond using boron trifluoride diethyl etherate (BF₃·OEt₂) as the fluorinating agent remains elusive. Conversely for phenoxylation, experimental and theoretical findings suggest an associative σ -bond metathesis mechanism for axial ligand exchanged between Cl-BsubPcs and phenols.⁵⁵

Converting axially chlorinated BsubPcs to axially fluorinated derivatives typically uses a large molar excess of BF₃·OEt₂ (upward of 25 equiv);^{53,56} but gram-scale reactions encounter stalling issues presumably due to concurrent equilibrium reactions between different boron trihalide species formed *in situ*.³⁶ Due to these limitations, our focus turned to silver tetrafluoroborate (AgBF₄), an alternative fluorinating agent offering benefits such as low stoichiometric excess (1.25 equiv of

AgBF₄), room temperature reaction conditions, and short reaction times (4 h).⁵⁷ Unlike hypothesized equilibrium reactions with BF₃·OEt₂, axial ligand exchange with AgBF₄ is driven by the precipitation of silver chloride.

We reacted **crude mixture 1a** with 2.50 equiv of AgBF₄ in anhydrous toluene at room temperature for 4.5 h (Scheme 4). We achieved full conversion of **crude mixture 1a** to the fully axially fluorinated **crude mixture 2a**, which was subjected to column chromatography and then train sublimation to isolate F-*Ph*₂-F₈Bsub(Pc₂-Nc₁) (**7b**) in 39% yield (Scheme 4).

Next, we introduced a phenoxy substituent in the axial position by modifying our established protocols for the axial phenoxylation of BsubPcs⁵⁸ and BsubNcs.⁵⁹ **Crude mixture 1a** was treated with 5 equiv of phenol (**8**) in refluxing 1,2-dichlorobenzene for 48 h to produce axially phenoxyated **crude mixture 3a** (Scheme 4). The change from commonly used toluene to 1,2-dichlorobenzene was prompted by the slow conversion in toluene even after 60 h of reflux, aligning with findings that electron-withdrawing groups in the periphery decrease axial phenoxylation kinetic rates.⁶⁰ We therefore selected 1,2-dichlorobenzene at a reaction temperature of 180 °C to accelerate the axial phenoxylation process. **Crude mixture 3a** was then subjected to column chromatography to isolate PhO-*Ph*₂-F₈Bsub(Pc₂-Nc₁) (**7c**) in 22% yield (Scheme 4). Train sublimation was not carried out in the purification of (**7c**) as we have previously observed instability of the boron–oxygen bond in sublimation conditions.⁶¹

2.4. Exploring the Reaction Scope

We investigated the mixed cyclotrimerization between 1,4-*Ph*₂-2,3-DCNP (**4**) and a variety of electronically different phthalonitriles to access a larger array of these hybrid macrocycles. We first attempted the reaction between (**4**) and 3,4,5,6-tetrachlorophthalonitrile (TCPN) (**6**) to form the peripherally chlorinated derivative of Cl-*Ph*₂-F₈Bsub(Pc₂-Nc₁) (**7a**), aiming to compare the impact of peripheral chlorine versus peripheral fluorine on the material properties of these hybrids. To our delight, the mixed cyclotrimerization between (**4**) and (**6**) under the same optimal reaction conditions (Entry 4, Table 1) resulted in the preferential formation of Cl-*Ph*₂-Cl₈Bsub(Pc₂-Nc₁) (**9a**) (Scheme 4) with an average HPLC MaxPlot peak area of 59% (based on triplicate experimental runs). Although the selectivity for (**9a**) was lower than that of (**7a**), the overall yield was higher at 29% and the only other significantly produced macrocycle in the crude mixture was Cl-Cl₁₂BsubPc (Figure 3c). The overall higher yield for (**9a**) is likely due to the larger separation in retention factors (*R*_f) of (**9a**) and Cl-Cl₁₂BsubPc on silica gel as the stationary phase in column chromatography. In the case of (**7a**), several mobile phases of varying polarities were tested on silica gel but the difference in *R*_f remained too small ($\Delta R_f < 0.2$) for adequate separation between (**7a**) and Cl-F₁₂BsubPc. In result, the total synthetic yields of hybrids (**7a**)–(**7c**) were less than anticipated since material coeluted with R_a-F₁₂BsubPc. Moreover, the mixed cyclotrimerization of 2,3-DCNP and (**6**) carried out under the same optimal reaction conditions (Entry 4, Table 1) significantly diminished selectivity for the Cl₈Bsub(Pc₂-Nc₁) hybrid and the primary macrocycle within this statistical distribution was Cl-Cl₁₂BsubPc (Figure 3c vs 3d). In our opinion, this further supports that selectivity for (**9a**) is the result of phenyl substituents in the 1,4- α,α' positions of 2,3-DCNP.

We further synthesized the axially fluorinated and axially phenoxyated derivatives of (**9a**) as comparison points in a complete array of bay-position phenylated, peripherally halogenated hybrids. Crude mixture **1b** was treated with 3.75 equiv of AgBF₄ in anhydrous toluene at room temperature for 6 h (Scheme 4). Higher equivalence of AgBF₄ and a longer reaction time were required due to solubility issues that arose when replacing the peripheral fluorine atoms with chlorine. (**9a**) displayed a sharp decrease in solubility and most of this macrocycle was collected as precipitated solids from the mixed cyclotrimerization of (**4**) and (**6**) (refer to the Supporting Information for details, the ¹H and ¹³C NMR spectra of hybrid (**9a**) could only be recorded in toluene-*d*₈). We were able to convert crude mixture **1b** to the fully axially fluorinated crude mixture **2b**, which was subjected to column chromatography and subsequent train sublimation to isolate F-*Ph*₂-Cl₈Bsub(Pc₂-Nc₁) (**9b**) in 42% yield (Scheme 4). For axial phenoxylation, crude mixture **1b** was reacted with 5 equiv of phenol (**8**) in refluxing 1,2-dichlorobenzene for 28 h to form PhO-*Ph*₂-Cl₈Bsub(Pc₂-Nc₁) (**9c**) within crude mixture **3b**. The latter mixture was subjected to column chromatography to isolate (**9c**) in 59% yield (Scheme 4).

2.5. Probing the Lewis Basicity of *o*-Dinitriles

In efforts to further expand the reaction scope, we attempted the BCl₃-templated mixed cyclotrimerization of 1,4-*Ph*₂-2,3-DCNP (**4**) with a series of less halogenated and non-halogenated phthalonitriles that are commercially available, mainly 4,5-difluorophthalonitrile (4,5-F₂PN) (**10**), 4,5-dichlorophthalonitrile (4,5-Cl₂PN) (**11**), and phthalonitrile (PN) (**12**) (Figure 4).

Several attempts were executed including the optimal reaction conditions above, but the mixed cyclotrimerizations with (**10**), (**11**), and (**12**) each resulted in mixtures primarily containing the C_{3v}-symmetric BsubPc and recovering most of the starting material (**4**). These results suggested a substantial lack in reactivity of (**4**) with this series of *o*-dinitriles (Tables S6–S8).

We moved onto determine whether differences in Lewis basicities could explain the selective reactivity of (**4**) with fully halogenated phthalonitriles compared to less halogenated and non-halogenated phthalonitriles in BCl₃-templated mixed cyclotrimerizations observed here. In the synthesis of BsubPcs, BsubNcs, and the broader phthalocyanine family, the interplay between the Lewis acidity of the metalloid/metal templating reagent and the Lewis basicity of the organic precursor can be crucial for macrocycle formation.⁶² This is well demonstrated by BsubPc formation at room temperature with BBr₃,⁵³ while the use of BCl₃ requires elevated temperatures.⁴⁰ To assess Lewis basicity, we computationally investigated the different *o*-dinitriles using DFT and the boron trifluoride (BF₃) affinity scale⁶³ with pyridine as a Lewis base due to it being extensively studied in this context (Figure 4a). These calculations were performed using the B3LYP functional with the 6-31G(d) basis set, known for good agreement with theoretical expectations.⁶²

In the following, the Lewis acidity of the boron templating reagent remains constant as that of BCl₃ which has been calculated elsewhere.⁶² The computed BF₃ affinities listed in Figure 4b indicate that *o*-dinitrile (**4**) has the highest Lewis basicity among the precursor materials studied herein, with a BF₃ affinity of 59.7 kJ/mol. Phthalonitriles (**5**) and (**6**) are low Lewis basicity reagents with BF₃ affinities of less than 51 kJ/mol. Conversely, the phthalonitriles whose BCl₃-templated mixed cyclotrimerizations with (**4**) were unsuccessful all have higher Lewis basicities ranging from 51.7 to 53.8 kJ/mol for (**11**), (**10**), and (**12**), in that order. The selective reactivity of (**4**) may arise from differences in the Lewis basicity of the participating precursor, complementing steric hindrance. Figure 4 illustrates an interactive balance of Lewis basicities, indicating that C_s-symmetric hybrids preferentially form from sterically driven mixed cyclotrimerizations employing an *o*-dinitrile with “high” Lewis basicity paired with another of “low” Lewis basicity. In other words, C_s-symmetric hybrids exhibit greater conversions and yields from a high–low Lewis basicity pairing compared to sterically driven cross-condensations using two *o*-dinitriles with similarly high Lewis basicities (i.e., high–high Lewis basicity pairing). For BCl₃-templated mixed cyclotrimerizations, we postulate that the interplay between the Lewis acidity of boron trichloride and the Lewis basicities of *o*-dinitrile precursors, along with the Lewis basicity balance between the two *o*-dinitrile precursors, are both key factors guiding hybrid macrocycle formation. Additional details on Lewis basicity calculations are in the Supporting Information.

2.6. Chemical Characterization of Hybrids (7a)–(7c) and (9a)–(9c)

All bay-position phenylated hybrids isolated in this work were characterized by 1D ¹H, ¹³C, and ¹¹B NMR along with 2D ¹H–¹H and ¹H–¹³C NMR. Hybrids containing fluorine, (**7a**)–(**7c**) and (**9b**), were further analyzed by 1D ¹⁹F, 2D ¹⁹F–¹⁹F, and 2D ¹⁹F–¹³C NMR. All NMR spectra are available in the Supporting Information.

For simplicity, we will compare the ¹H NMR spectra of Cl-*Ph*₂-F₈Bsub(Pc₂-Nc₁) (**7a**) and Cl-*Ph*₂-Cl₈Bsub(Pc₂-Nc₁) (**9a**) which both bear an axial chloride but differ in their peripheral

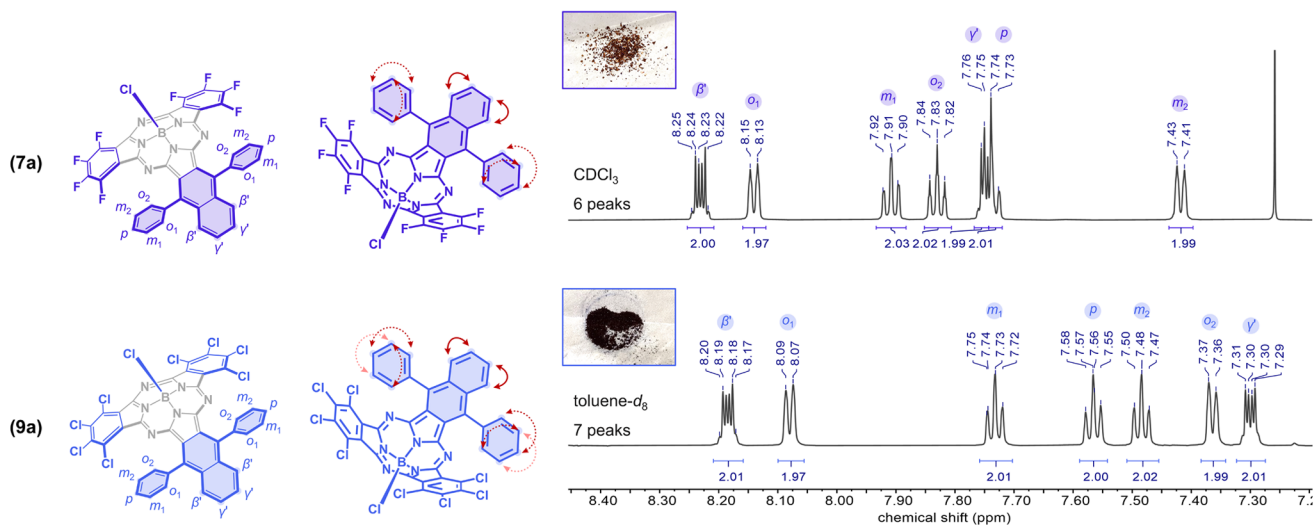
| 1D, 2D COSY, and 2D TOCSY ¹H NMR Signals


Figure 5. Stacked ¹H NMR spectra of peripherally fluorinated Cl-Ph₂-F₈Bsub(PC₂-Nc₁) (7a) in CDCl₃ (top) and peripherally chlorinated Cl₈Bsub(PC₂-Nc₁) (9a) in toluene-*d*₈ (bottom). 2D ¹H-¹H gCOSY (solid arrows) and 2D ¹H-¹H TOCSY (dashed arrows) interactions are shown in red (refer to Figures S76–S79 and Figures S121–S124 for 2D ¹H-¹H NMR spectra). ¹H NMR data shown here and photographs of materials (insets) were acquired from train sublimed samples.

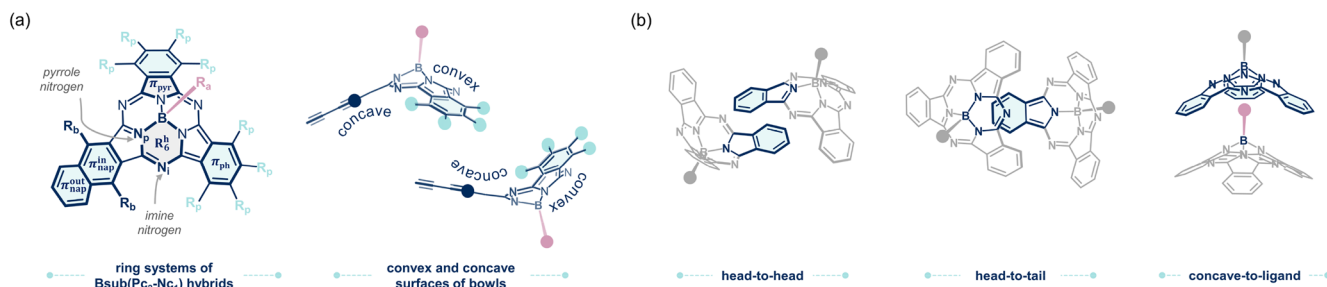
 | Solid-state Nomenclature & Interactions of BsubPc-related Compounds


Figure 6. (a) Atom and fragment identification of the Bsub(PC₂-Nc₁) macrocycle and orientation of the convex and concave surfaces. (b) Common solid-state intermolecular interactions among neighboring BsubPcs indicated by the relative position of isoindole groups (highlighted: head-to-head, head-to-tail, and concave-to-ligand).

motif of fluorination versus chlorination, respectively. Additionally, we compared the axially chlorinated hybrids since the relative insolubility of (9a) in deuterated chloroform allowed us to discern differences in peak resolution between CDCl₃ and toluene-*d*₈. With respect to ¹H NMR, we observed six well-resolved proton peaks for (7a) in CDCl₃ whereas seven well-resolved proton peaks were observed for (9a) in toluene-*d*₈, resulting in one peak per chemically equivalent proton pair and each peak integrating to two protons (Figure 5). The splitting patterns for the seven well-resolved peaks include two multiplets, two doublets, and three triplets.

Moreover, the C_s-symmetry plane bisects the naphthalene unit of Ph₂-(R_p)₈Bsub(PC₂-Nc₁) hybrids and makes the respective hydrogen atoms in the β' and γ' positions chemically equivalent, giving rise to a pair of multiplets with signal splitting indicative of long-range coupling (Figure 5). Diagnostic deshielded signals near 8.20 ppm correspond to the β' protons for both peripherally fluorinated (7a) and peripherally chlorinated (9a).

The ¹H NMR spectra of these hybrid macrocycles were carefully assigned by 2D ¹H-¹H gCOSY and 2D ¹H-¹H TOCSY NMR spectroscopy. The bay-position phenyl sub-

stituents are further bisected by an axis perpendicular to the C_s-symmetry plane resulting in two pairs of *ortho*-protons (o₁ and o₂), two pairs of *meta*-protons (m₁ and m₂), and one pair of *para*-protons (p). ¹H-¹H gCOSY NMR for (7a) shows a single coupling interaction between protons at 7.75 ppm (γ') and 8.24 ppm (β'), validating that γ' and β' are neighboring vicinal protons on the naphthalene subunit (Figures S76 and S77). This is also confirmed for (9a) whose ¹H-¹H gCOSY NMR spectrum indicates a strong coupling between protons at 7.30 ppm (γ') and 8.19 ppm (β') (Figures S121 and S122). For the phenyl groups, ¹H-¹H TOCSY NMR spectra show moderate signals for long-range coupling of protons two bonds away and weaker signals for protons three bonds away (Figures S78, S79, S123, and S124). ¹H-¹H gCOSY and ¹H-¹H TOCSY NMR were analyzed together to confirm assignments for sets of phenyl group signals with similar splitting patterns and proton integrations.

2.7. X-ray Crystal Structure Analysis

There are two general classifications of BsubPc solid-state arrangements that have been previously outlined.^{65,66} One method describes the interaction between the bowl shapes of individual molecules (Figure 6a), while the other explains the

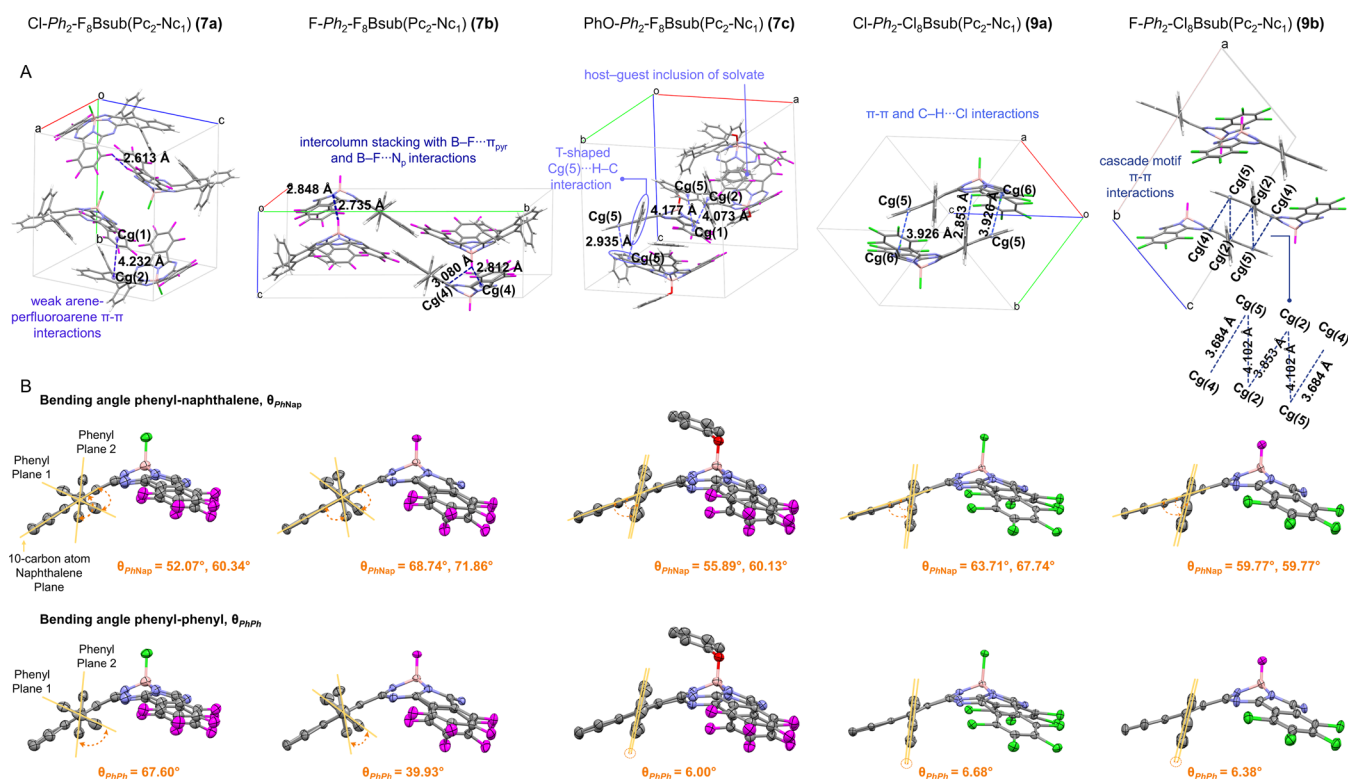


Figure 7. (A) Unit cell sections of (7a)—CCDC 2305677, (7b)—CCDC 2305678, (7c)—CCDC 2305679, (9a)—CCDC 2305680, and (9b)—CCDC 2305681 with select intermolecular interactions, centroids, and distances labeled. Solvate molecules are omitted for clarity except for (7c). (B) ORTEP structures of (7a), (7b), (7c), (9a), and (9b) with thermal ellipsoids at 50% probability and bending angles θ_{PhNap} , θ_{PhPh} . Hydrogen atoms are removed for clarity. Colors: carbon—gray, hydrogen—white, nitrogen—blue, boron—light pink, chlorine—green, fluorine—magenta, oxygen—red.

alignment of isoindole groups between neighboring BsubPcs (Figure 6b).

All X-ray diffractable single crystals reported herein were obtained either by solvent crystallization methods or by previously described⁶⁷ train sublimation methods. Solubility differences between the peripherally fluorinated and peripherally chlorinated hybrids raised issues in obtaining single crystals of all six hybrids from one consistent crystal growth process. Single crystals of Cl-*Ph*₂-F₈Bsub(PC₂-NC₁) (7a) were obtained by train sublimation. Slow vapor diffusion with benzene/heptane allowed growth of F-*Ph*₂-F₈Bsub(PC₂-NC₁) (7b) and PhO-*Ph*₂-F₈Bsub(PC₂-NC₁) (7c) single crystals, whereas slow vapor diffusion with toluene/heptane formed single crystals of Cl-*Ph*₂-Cl₈Bsub(PC₂-NC₁) (9a) and F-*Ph*₂-Cl₈Bsub(PC₂-NC₁) (9b). X-ray quality crystals of PhO-*Ph*₂-Cl₈Bsub(PC₂-NC₁) (9c) could not be obtained by slow vapor diffusion, even after numerous attempts.

(7a) arranges in a monoclinic crystal system with a $P2_1/c$ space group and 4 molecules in the unit cell (Table S9, Figure 7A). The molecules in the unit cell exhibit peripheral fluorine-fluorine interactions between two neighboring Bsub(PC₂-NC₁)s with separation distances ranging from 2.613–3.381 Å. Weak concave-concave arene-perfluoroarene interactions are also present between a peripherally fluorinated isoindole fragment (π_{ph}) of one molecule and the inner ring of the benz(f)isoindole fragment (π_{nap}^{in}) of a neighboring molecule, separated by a ring centroid distance Cg(1)⋯Cg(2) of 4.232 Å. (7a) exhibits an atypically distorted concave-concave head-to-head arrangement driven mainly by weak arene-perfluoroarene interactions.

The (7b) single crystal is also a monoclinic system with 4 molecules in the unit cell and a $P2_1/c$ space group. There is half

of a benzene solvent molecule (0.5C₆H₆) in the unit formula, and this solvate is incorporated into the corners of the unit cell (Table S9). Despite the bulky bay-position phenyl groups, the small atomic size of fluorine enables a column-like stacking of (7b) through B-F⋯ π_{pyr} interactions at distances ranging from 2.812–3.080 Å with centroid Cg(4) (Figure 7A). The axial fluoride also interacts with each of the pyrrole nitrogens (B-F⋯N_p) at separation distances ranging between 2.735 and 2.848 Å. This concave-to-axial halide conformation is consistent with that of axially and peripherally fluorinated F-F₆BsubPc and F-F₁₂BsubPc.⁵⁶

Grown from the same slow vapor diffusion process as (7b), the (7c) single crystal is an orthorhombic system with a $Pnna$ space group and 8 molecules in the unit cell. The solution-grown crystal of (7c) contains a benzene solvent molecule which is disordered about a 2-fold rotation axis giving 0.5C₆H₆ in the unit formula (Table S9). Interestingly, the benzene solvate occupies the concave bowl cavity of two Bsub(PC₂-NC₁)s in a host-guest type of arrangement.⁶⁶ The key interactions between neighboring (7c) molecules include concave-concave T-shaped interactions between the outer 6-membered ring of the benz(f)isoindole fragment (π_{nap}^{out}) of one molecule and the bay-position phenyl group of a neighboring molecule [Cg(5)⋯H-C] at a distance of 2.935 Å (Figure 7A). We also note weak convex-convex head-to-head arene-perfluoroarene interactions at ring centroid distances Cg(1)⋯Cg(2) and Cg(1)⋯Cg(5) of 4.073 and 4.177 Å, respectively. Unlike the single crystal of (7b) featuring an axial fluoride, the larger phenol moiety facilitates solvent incorporation between the concaving bowls of (7c) molecules.

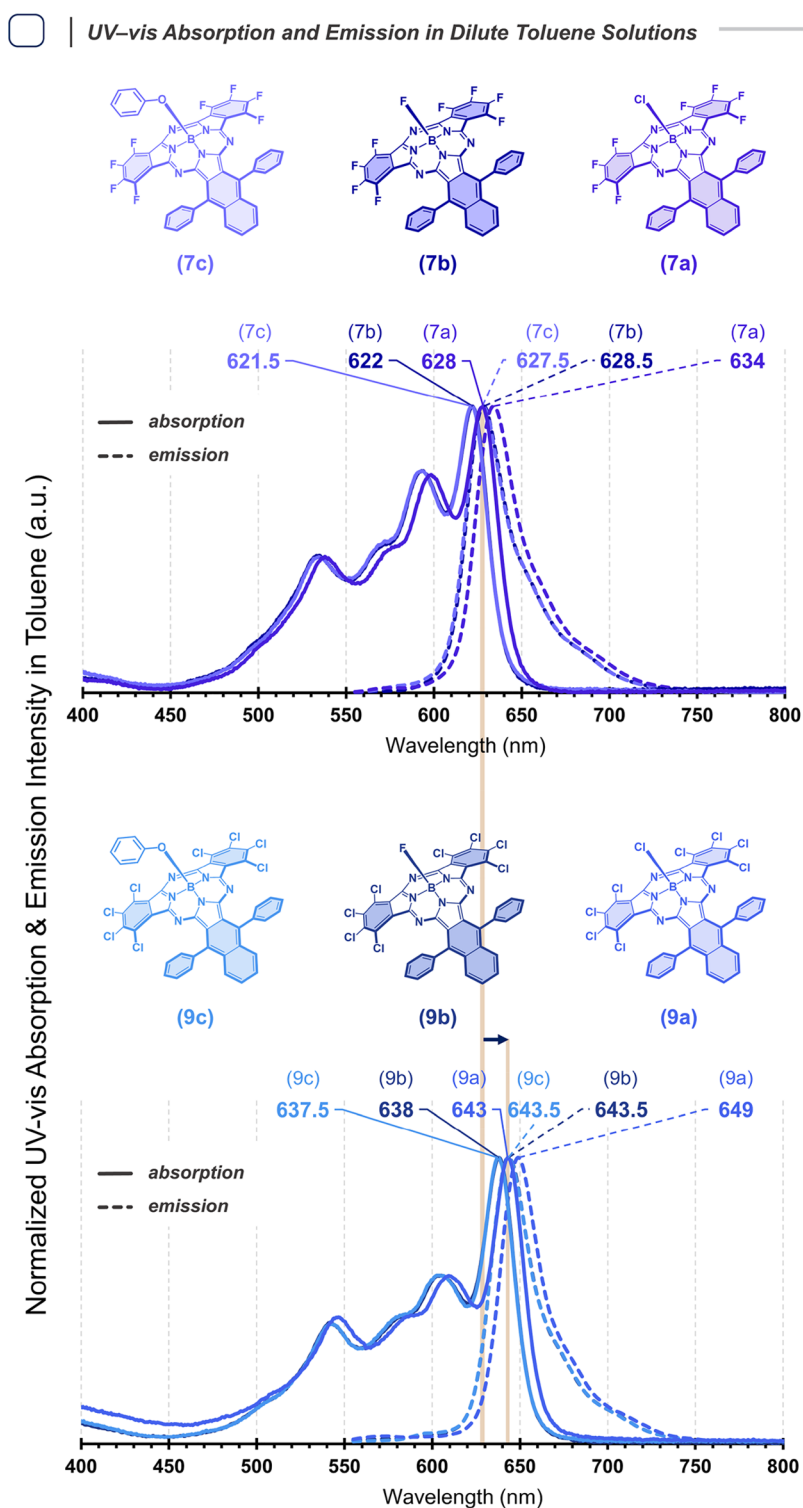
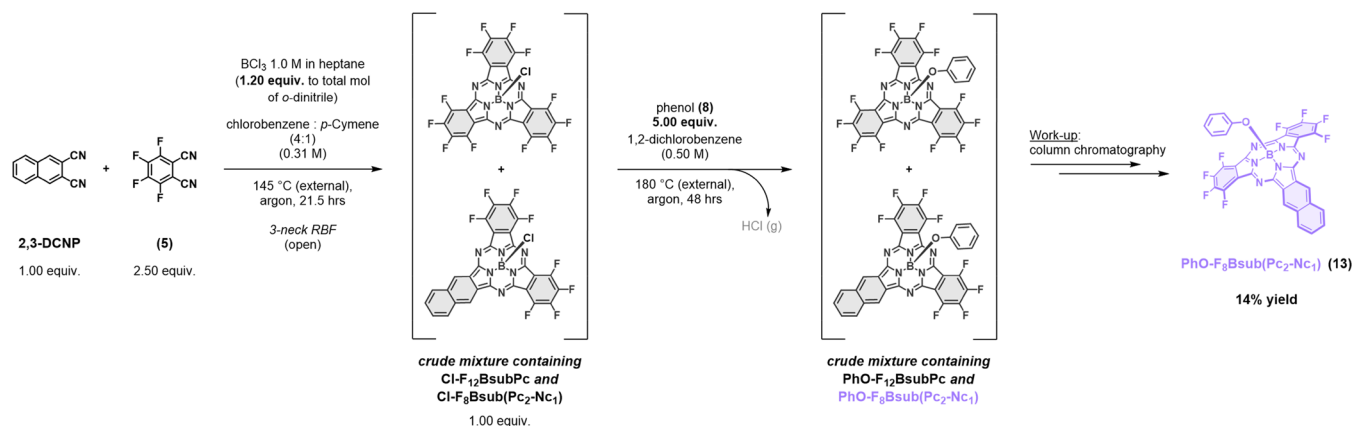


Figure 8. Stacked and normalized UV-vis absorption (solid lines) and emission (dashed lines) spectra of Cl- (7a), F- (7b), and PhO-*Ph*₂-F₈Bsub(Pc₂-Nc₁) (7c) along with Cl- (9a), F- (9b), and PhO-*Ph*₂-Cl₈Bsub(Pc₂-Nc₁) (9c) hybrids in toluene at room temperature. All compounds were excited with a wavelength (λ_{ex}) of 535 nm. All absorption and emission data were acquired from train sublimed samples except for the axially phenoxyolated hybrids (7c) and (9c) which were purified by column chromatography.

Considering the single crystals of peripherally chlorinated hybrids grown via the toluene/heptane diffusion method, (9a) was found to arrange in a triclinic system with a *P*-1 space group and 1 molecule in the unit cell (Table S9). The solution-grown crystal of (9a) contains half a molecule of heptane for each main molecule in the unit cell, with heptane occupying the corners of

the unit cell. In the solid state, (9a) molecules arrange with concave-concave π - π interactions between the $\pi_{\text{nap}}^{\text{out}}$ ring of one molecule and the peripherally chlorinated isoindole fragment (π_{ph}) of another molecule, separated by a ring centroid distance of 3.926 Å [Cg(5)⋯Cg(6)] (Figure 7A). Similar close-packing π - π interactions have been observed in other axially and

Scheme 5. Synthetic Route for PhO-F₈Bsub(PC₂-NC₁) (13) in the Context of This Work^a

^aCrude mixture containing Cl-F₁₂BsubPc and Cl-F₈Bsub(PC₂-NC₁) was synthesized following Method S.6 from our previous work.³⁶

peripherally chlorinated BsubPcs such as Cl-Cl₆BsubPc and Cl-Cl₁₂BsubPc.^{66,68} (9a) also exhibits C–H⋯Cl bonds at 2.853 and 2.907 Å with the bay-position phenyl groups and 6-membered $\pi_{\text{nap}}^{\text{out}}$ ring, respectively.

On the other hand, the single crystal of (9b) arranges in a monoclinic system with a *C2/m* space group and 4 molecules in the unit cell (Table S9). The SQUEEZE routine was used to remove the toluene solvate from the data as its disordered nature was inhibiting structure refinement, creating voids in the unit cell where the solvent would appear. Notably, (9b) exhibits an orderly solid-state packing consisting of convex–convex head-to-head π – π interactions between the benz(*f*)isoindole fragments of two neighboring molecules. This close-packing arrangement displays a cascade motif of π – π interactions that can be described as $\pi_{\text{pyr}} \cdots \pi_{\text{nap}}^{\text{out}} \cdots \pi_{\text{nap}}^{\text{out}} \cdots \pi_{\text{nap}}^{\text{in}} \cdots \pi_{\text{nap}}^{\text{in}} \cdots \pi_{\text{nap}}^{\text{in}} \cdots \pi_{\text{nap}}^{\text{in}} \cdots \pi_{\text{nap}}^{\text{out}} \cdots \pi_{\text{pyr}}$ with ring centroid distances Cg(4)⋯Cg(5), Cg(5)⋯Cg(2), Cg(2)⋯Cg(2), Cg(2)⋯Cg(5), and Cg(5)⋯Cg(4) of 3.684, 4.102, 3.853, 4.102, and 3.684 Å, respectively (Figure 7A).

Across this array of hybrids, a consistent trend was observed where bay-position phenyl groups were either in a crisscross or parallel orientation to each other, but always oblique to the naphthalene subunit of the macrocyclic scaffold (Figure 7B). These orientations were assessed by determining the phenyl-naphthalene bending angle (θ_{PhNap}), which is the angle between each phenyl group (6-carbon atom plane) and the 10-carbon atom naphthalene plane, and the phenyl–phenyl bending angle (θ_{PhPh}), which is the angle between Phenyl Plane 1 and Phenyl Plane 2 (Figure 7B, Table S10). The θ_{PhNap} values varied widely for the peripherally fluorinated (7a)–(7c) series at 52.1–71.9°, compared to the peripherally chlorinated hybrids (9a) and (9b) at 59.8–67.7°, with (7b) displaying angles closest to orthogonality. Interestingly, among the solvent-grown crystals, only (7b) exhibited a crisscross phenyl group orientation ($\theta_{\text{PhPh}} = 39.9^\circ$), whereas (7c), (9a), and (9b) each featured parallel-aligned phenyl groups ($\theta_{\text{PhPh}} = 6.0$ – 6.7°). Moreover, (9b) showcased the synergistic benefit of incorporating rigid bay-position phenyl groups, a small axial fluorine, and large vdW radii of peripheral chlorine atoms for crafting a well-ordered close-packing arrangement.

2.8. Photophysical Properties and Spectroscopy Analysis

The ultraviolet–visible (UV–vis) absorption and photoluminescence (PL) spectra of (7a)–(7c) and (9a)–(9c) hybrids in diluted toluene solutions are illustrated in Figure 8.

For an additional comparison point, PhO-F₈Bsub(PC₂-NC₁) (13), synthesized in this study (Scheme 5), was incorporated into the hybrid array to elucidate the influence of axial functionalization (chlorination vs fluorination vs phenoxylation) and the impact of phenyl groups in the bay positions on the material properties of peripherally fluorinated F₈Bsub(PC₂-NC₁) hybrids. Figure 8 depicts splitting of the Q band in *Ph*₂-(R_p)₈Bsub(PC₂-NC₁) hybrids, consistent with our prior work on F₈Bsub(PC₂-NC₁)s.³⁶ The UV–vis spectra exhibit the characteristic broad absorption with full width at half-maximum height (fwhm^{abs}_{sol}) between 54.5–66 nm, featuring well-resolved shoulder peaks of higher energy at ≈ 30 , ≈ 50 , and ≈ 90 nm blue-shifted from the maximum absorption peak ($\lambda_{\text{max, sol}}^{\text{abs}}$) (Table 2). The peripherally chlorinated (9a)–(9c) hybrids show a 15–16 nm red-shift in $\lambda_{\text{max, sol}}^{\text{abs}}$ compared to the peripherally fluorinated (7a)–(7c) series, aligning with their smaller band gaps of 1.87–1.89 eV. This mirrors trends in C_{3v}-symmetric peripherally halogenated BsubPcs⁵⁶ and in other related compounds, such as porphyrins and phthalocyanines,⁶⁹ where peripheral chlorines red-shift absorption spectra and peripheral fluorines have a blue-shift effect. The UV–vis absorption spectra show minor shifts (5–6 nm blue-shift) between axial Cl– and axial F– and negligible shifts (0.5 nm) between axial F– and axial PhO–. These trends align with previous observations for F₈Bsub(PC₂-NC₁) hybrids,³⁶ highlighting minimal alteration in photophysical properties due to axial ligand substitution, particularly in absorption band position.^{56,70}

Upon excitation ($\lambda_{\text{ex}} = 535$ nm), intense and narrow emission peaks were observed for diluted toluene solutions of (7a)–(7c) and (9a)–(9c) hybrids (Figure 8). The emission maxima ($\lambda_{\text{max, sol}}^{\text{PL}}$) were gradually bathochromically shifted from 627.5–634.0 to 643.5–649.0 nm for (7a)–(7c) to (9a)–(9c), illustrating the fine-tuning of color from near-red to red by increasing the peripheral halogen size of these *Ph*₂-(R_p)₈Bsub(PC₂-NC₁) hybrid emitters. The fwhm_{sol}^{PL} values and Stokes shifts of (7a)–(7c) (30–31 nm and 151–166 cm⁻¹) and (9a)–(9c) (28.5–29 nm and 134–146 cm⁻¹) were remarkably small, indicating a narrow LUMO density of states and high structural rigidity of these C_s-symmetric macrocycles. The significantly small Stokes shifts are consistent with photophysical results reported for F₈Bsub(PC₂-NC₁) hybrids,³⁶ and for other BsubPcs⁵⁶ and BsubNcs.⁵⁹

Table 2. Photophysical Properties of R₄-P/I₂-(R_p)₈Bsub(Pc₂-Nc₁) Hybrids Presented Herein and R₄-F₈Bsub(Pc₂-Nc₁) Hybrids Studied in Our Previous Work^a

compound	maximum absorption wavelength, $\lambda_{\text{max,abs}}^{\text{abs}}$ (nm)	maximum emission wavelength, $\lambda_{\text{max,em}}^{\text{PL}}$ (nm)	fwhm ^{abs} (nm; cm ⁻¹)	fwhm ^{PL} (nm; cm ⁻¹)	optical band gap, E_g^{opt} (eV) ^b	Stokes shift (nm; cm ⁻¹)	Φ_{PL} in toluene (%) ^c		
							F ₃ PhO-BsubPc reference fluorophore ^d	PhO-F ₁₂ BsubPc reference fluorophore ^e	Cresyl Violet perchlorate reference fluorophore ^f
Cl-P/I ₂ -F ₈ Bsub(Pc ₂ -Nc ₁) (7a)	628	634	63; 1715	31; 763	1.92	6; 151			
F-P/I ₂ -F ₈ Bsub(Pc ₂ -Nc ₁) (7b)	622	628.5	65; 1811	30; 752	1.93	6.5; 166	14	15	16
PhO-P/I ₂ -F ₈ Bsub(Pc ₂ -Nc ₁) (7c)	621.5	627.5	66; 1842	30; 753	1.94	6; 154	12	13	13
Cl-P/I ₂ -Cl ₈ Bsub(Pc ₂ -Nc ₁) (9a)	643	649	55; 1404	28.5; 672	1.87	6; 144			
F-P/I ₂ -Cl ₈ Bsub(Pc ₂ -Nc ₁) (9b)	638	643.5	54.5; 1415	29; 695	1.89	5.5; 134	12	12	11
PhO-P/I ₂ -Cl ₈ Bsub(Pc ₂ -Nc ₁) (9c)	637.5	643.5	55.5; 1443	29; 695	1.89	6; 146	9	10	9
Cl-F ₈ Bsub(Pc ₂ -Nc ₁) ^g	618	622.5	53; 1468	25; 640	1.95	4.5; 117			
F-F ₈ Bsub(Pc ₂ -Nc ₁) ^g	614	618	55; 1560	25.5; 663	1.96	4; 105	17	22	24
PhO-F ₈ Bsub(Pc ₂ -Nc ₁) (13)	613	618	60; 1716	26; 677	1.97	5; 132	13	18	20

^aSolution-state measurements were acquired in toluene at room temperature. fwhm = full width at half-maximum height. ^bEstimated from the absorption spectrum specifically at the intersection of the baseline and the tangent line from where absorption onset occurs using the equation $E_g^{\text{opt}} = 1240/\lambda_{\text{onset}}^{36}$. ^cMeasured in dilute toluene solutions and determined using the relative quantum yield method. ^d $\lambda_{\text{ex}} = 521$ nm. ^e $\lambda_{\text{ex}} = 532$ nm. ^f $\lambda_{\text{ex}} = 536$ nm. ^gFrom our previous publication about R₄-F₈Bsub(Pc₂-Nc₁) hybrids.³⁶

□ | Electrochemical Properties

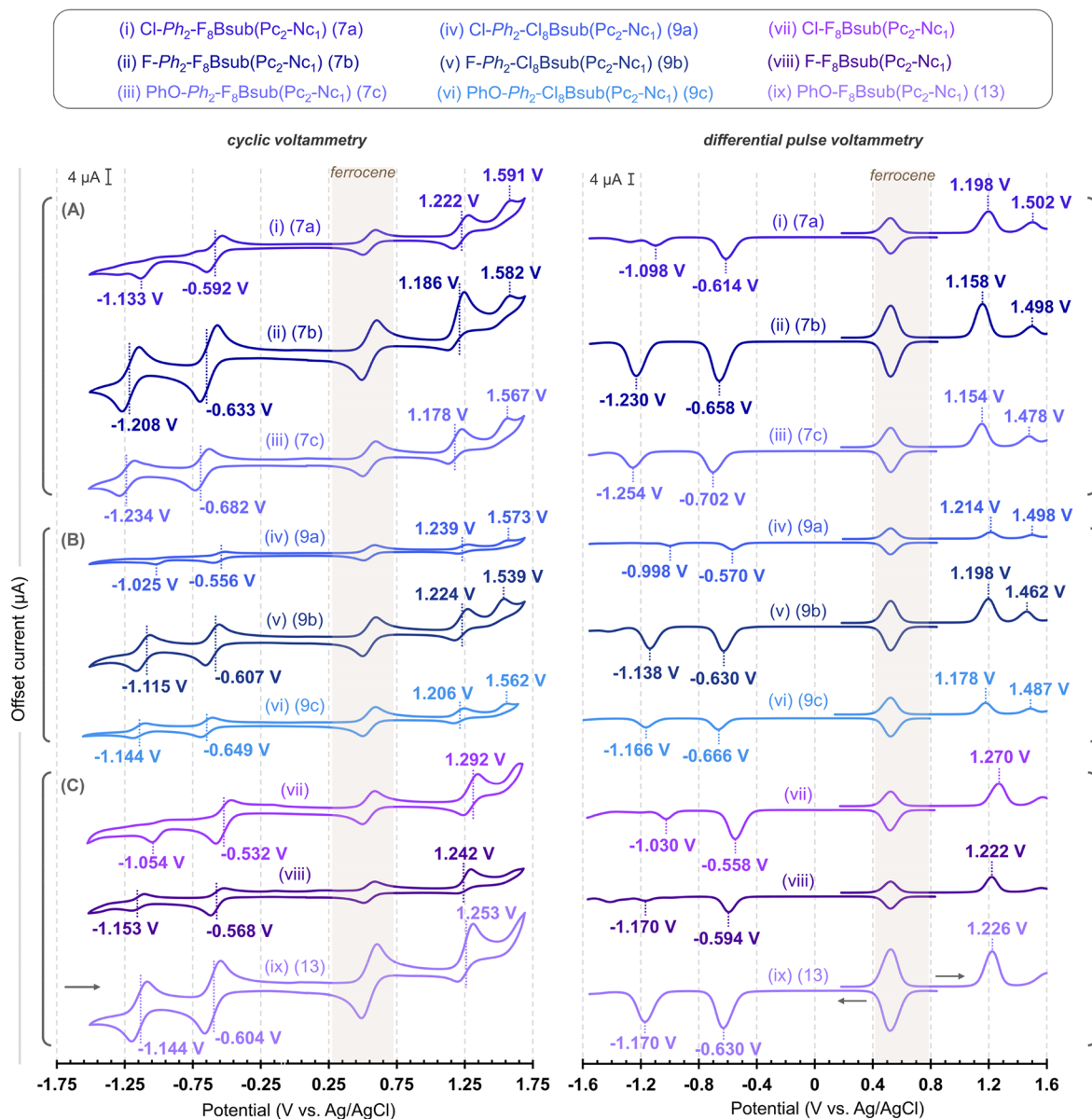


Figure 9. Cyclic voltammograms (left) and differential pulse voltammograms (right) of (A) bay-position phenylated F₈ hybrids (i) (7a), (ii) (7b), (iii) (7c); (B) bay-position phenylated Cl₈ hybrids (iv) (9a), (v) (9b), (vi) (9c) along with (C) peripherally fluorinated F₈ hybrids (vii) Cl-F₈Bsub(PC₂-NC₁), (viii) F-F₈Bsub(PC₂-NC₁), and (ix) (13) as comparison points. Conditions: 0.1 M tetrabutylammonium perchlorate as the electrolyte solution in nitrogen-degassed dichloromethane at room temperature with a 100 mV s⁻¹ scan rate and ferrocene/ferrocenium (Fc/Fc⁺; E_{1/2,ox} = 0.547 V vs Ag/AgCl) as an internal reference.

Furthermore, the absorption and emission maxima of *Ph*₂-F₈Bsub(PC₂-NC₁) hybrids are red-shifted compared to their F₈Bsub(PC₂-NC₁) counterparts (Table 2), indicating increased π -conjugation in the peripheral motif due to bay-position phenyl groups. This red-shift, however, is less pronounced than that observed for the additional fused benzo ring in F₈Bsub(PC₂-NC₁)s compared to F₈BsubPcs.³⁶ The orientation of bay-position phenyl groups in a more oblique rather than parallel fashion to the naphthalene subunit (Figure 7B) results in less *p*-orbital overlap, limiting π -system enlargement required for a significant red-shift effect.

2.9. Relative Photoluminescence Quantum Yields

The fluorescence efficiency of bay-position phenylated hybrids (7b), (7c), (9b), and (9c) was assessed by measuring the relative photoluminescence quantum yield (QY, Φ_{PL}).⁷¹ Axially chlorinated hybrids (7a) and (9a) were omitted from the Φ_{PL} analysis due to small amounts of axially hydrolyzed impurities (i.e., 0.42–1.40% peak areas on HPLC MaxPlots) present in each sample. The general method for calculating the relative Φ_{PL} in dilute solution is described in the Supporting Information. Table 2 lists the relative Φ_{PL} values calculated using each of the three reference fluorophores as outlined in our previous work on F₈Bsub(PC₂-NC₁)s.³⁶ Comparing all reference fluorophores, the QY values are lowest for the Cl₈ hybrids (9b) (11–12%) and (9c) (9–10%), likely due to the heavy atom effect promoting

Table 3. Electrochemical and Electronic Properties of Bay-Position Phenylated $Ph_2-(R_p)_8Bsub(Pc_2-Nc_1)$ and $F_8Bsub(Pc_2-Nc_1)$ Hybrids Including Cyclic Voltammetry, Differential Pulse Voltammetry, Solution UV–vis Spectroscopy Methods, and Density Functional Theory (DFT) Modeling

compound	cyclic voltammetry					differential pulse voltammetry				UV–vis spectroscopy			DFT modeling	
	oxidation		reduction			oxidation		reduction		solution UV–vis	estimated frontier orbital energies		B3P86/6-311G ^f	
	$E_{1/2,ox}^1$ (V)	$E_{p,a}$ (V)	$E_{1/2,red}^1$ (V)	$E_{1/2,red}^2$ (V)	$E_{p,c}$ (V)	E_{pa}^1 (V) ^c	E_{pa}^2 (V) ^c	E_{pc}^1 (V) ^c	E_{pc}^2 (V) ^c	E_g^{opt} (eV)	HOMO (eV) ^d	LUMO (eV) ^e	HOMO (eV)	LUMO (eV)
Cl- Ph_2 - $F_8Bsub(Pc_2-Nc_1)$ (7a)	1.222	1.591 ^b	−0.592		−1.133 ^b	1.198	1.502	−0.614	−1.098	1.92	−6.11	−4.19	−5.94	−4.17
F- Ph_2 - $F_8Bsub(Pc_2-Nc_1)$ (7b)	1.186 ^a	1.582 ^b	−0.633	−1.208		1.158	1.498	−0.658	−1.230	1.93	−6.06	−4.13	−5.94	−4.13
PhO- Ph_2 - $F_8Bsub(Pc_2-Nc_1)$ (7c)	1.178	1.567 ^b	−0.682	−1.234		1.154	1.478	−0.702	−1.254	1.94	−6.05	−4.11	−5.85	−4.05
Cl- Ph_2 - $Cl_8Bsub(Pc_2-Nc_1)$ (9a)	1.239	1.573 ^b	−0.556		−1.025 ^b	1.214	1.498	−0.570	−0.998	1.87	−6.13	−4.26	−5.90	−4.12
F- Ph_2 - $Cl_8Bsub(Pc_2-Nc_1)$ (9b)	1.224	1.539 ^b	−0.607	−1.115		1.198	1.462	−0.630	−1.138	1.89	−6.11	−4.22	−5.87	−4.07
PhO- Ph_2 - $Cl_8Bsub(Pc_2-Nc_1)$ (9c)	1.206	1.562 ^b	−0.649	−1.144		1.178	1.487	−0.666	−1.166	1.89	−6.09	−4.20	−5.83	−4.02
Cl- $F_8Bsub(Pc_2-Nc_1)$ ^g	1.292		−0.532		−1.054 ^b	1.270		−0.558	−1.030	1.95	−6.20	−4.25	−6.13	−4.28
F- $F_8Bsub(Pc_2-Nc_1)$ ^g	1.242 ^a		−0.568	−1.153		1.222		−0.594	−1.170	1.96	−6.13	−4.17	−6.09	−4.23
PhO- $F_8Bsub(Pc_2-Nc_1)$ (13)	1.253		−0.604	−1.144		1.226		−0.630	−1.170	1.97	−6.15	−4.18	−6.02	−4.15

^aQuasi-reversible. ^bIrreversible. ^cMaximum peak potential from DPV scans. ^dEstimated using the first oxidation half-wave potential and the equation developed by D'Andrade et al.⁷⁶ ^eEstimated by adding the calculated solution UV–vis band gap energy (E_g^{opt}) to the estimated HOMO energy. ^fCalculated at the B3P86/6-311G level and calibrated using the respective formulas developed by Holst et al.⁷⁷ ^gFrom our previous publication on R_a - $F_8Bsub(Pc_2-Nc_1)$ hybrids.³⁶

fast intersystem crossing.^{28,72,73} The axially fluorinated hybrids (7b) and (9b) exhibit slightly higher QYs by 2–3% than their axially phenoxyated counterparts (7c) and (9c). Additionally, QY values for (7b) (14–16%) and (7c) (12–13%) were consistently lower than those for nonbay-position phenylated $F_8Bsub(Pc_2-Nc_1)$ (17–24%)³⁶ and (13) (13–20%), suggesting energy losses in nonradiative deactivation processes such as vibrational relaxation of the unfused phenyl groups.

2.10. Electrochemical Analysis

To further evaluate the impact of bay-position phenyl groups and axial/peripheral functionalization on the material properties of $Bsub(Pc_2-Nc_1)$ hybrids, cyclic voltammetry (CV), differential pulse voltammetry (DPV), and DFT computational studies were conducted. The bay-position phenylated hybrids (7a)–(7c) and (9a)–(9c) exhibited a reversible first oxidation potential ($E_{1/2,ox}^1$) around 1.2 V, except for (7b) whose $E_{1/2,ox}^1$ was quasi-reversible, along with an irreversible second oxidation potential above 1.5 V. On the reduction side, these hybrid macrocycles were more stable: reversible one-electron ($E_{1/2,red}^1$) and two-electron ($E_{1/2,red}^2$) processes were obtained for all six bay-position phenylated hybrids except for axially chlorinated (7a) and (9a), which each exhibited an irreversible, second reduction potential ($E_{p,c}$) at −1.133 and −1.025 V, respectively (Figure 9A,B). In terms of peripheral trends, chlorine atoms in the periphery facilitate the reduction process with (9a)–(9c) hybrids having higher reduction potentials and increased stability toward oxidation compared to (7a)–(7c) hybrids. DPV results show analogous trends to CV, with first and second reduction potentials increasing with chlorination in the periphery. The 26–36 mV anodic shift in $E_{1/2,red}^1$ for Cl_8 hybrids (9a)–(9c) suggests superior electron acceptor capacity in organic electronics compared to their F_8 counterparts (7a)–

(7c), consistent with observations in peripherally trichlorinated $BsubPcs$.⁷⁴

Regarding the axial ligand effect on redox potentials, an electron-withdrawing fluorine or aromatic-based phenol substituent enhanced electrochemical reversibility in the reduction regime, significantly improving the stability of reduced states in Ph_2 - $F_8Bsub(Pc_2-Nc_1)$ s and Ph_2 - $Cl_8Bsub(Pc_2-Nc_1)$ s. This is crucial for the longevity of organic electronic devices undergoing repeated redox cycles, aligning with previous findings on axially fluorinated $BsubPcs$ ⁷⁵ and $F_8Bsub(Pc_2-Nc_1)$ hybrids.³⁶

Phenyl substituents in the bay positions lowered first oxidation potentials of hybrids (7a)–(7c) by 56–75 mV compared to their R_a - $F_8Bsub(Pc_2-Nc_1)$ counterparts (Table 3). Interestingly, the added aromaticity from phenyl substituents modestly improved electrochemical reversibility in reduction for hybrids (7a)–(7c) but not in oxidation (Figure 9A,C). This suggests that the slightly more π -extended diphenyl-substituted benz(*f*)isoindole units better stabilize the (R_b)_y- $F_8Bsub(Pc_2-Nc_1)$ hybrid in its reduced states than in its oxidized states. Further derivatives, especially unsubstituted ones without peripheral halogenation, are required to assess the broader influence of bay-position phenyl groups on this class of materials.

Furthermore, CV and DPV results aligned well with estimated frontier orbital energies listed in Table 3. Analysis of estimated HOMO and LUMO levels showed slightly higher HOMO energy levels for peripherally fluorinated hybrids (7a)–(7c), making them easier to oxidize. Conversely, lower-lying LUMO levels indicated easier reduction for the peripherally chlorinated (9a)–(9c) series. Computed HOMO and LUMO values agreed with trends observed for axial ligand effects, reflecting a staircase pattern from axial B–Cl bonds (facilitated reduction) to axial B–OPh bonds (easier oxidation) (Figure 10). DFT calculations

Computational HOMO–LUMO Levels and Band Gap Energies

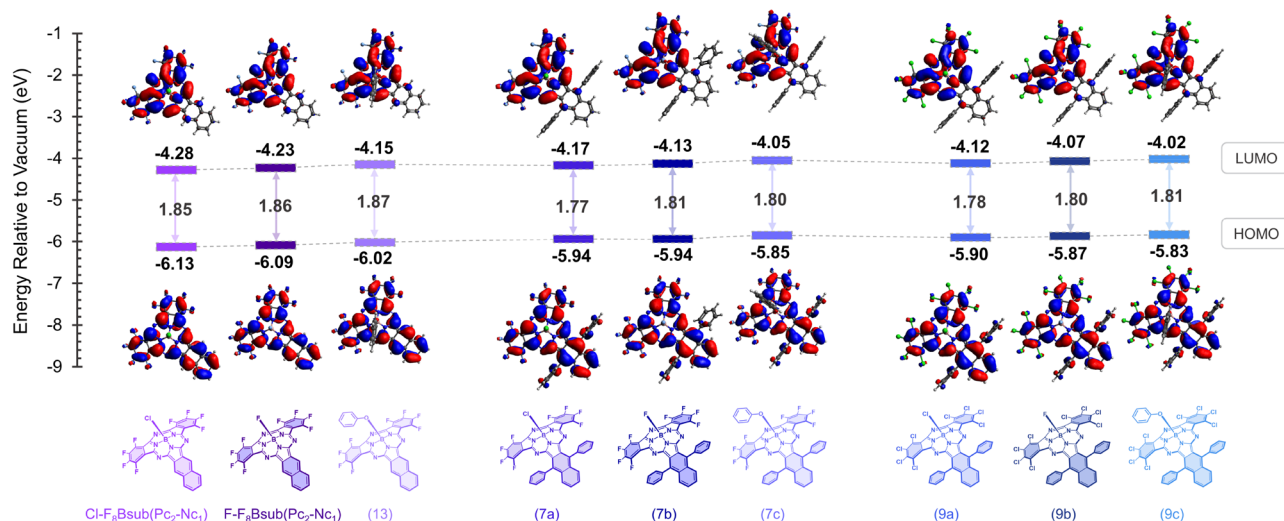


Figure 10. Molecular orbitals calculated at the B3P86/6-311G level and calibrated⁷⁷ for F₈Bsub(PC₂-Nc₁)s, Ph₂-F₈Bsub(PC₂-Nc₁)s, and Ph₂-Cl₈Bsub(PC₂-Nc₁)s in order of axial substituent: chloro, fluoro, and phenoxy.

in Figure 10 illustrate the delocalization of HOMOs over the entire aromatic framework whereas LUMOs were centralized over the macrocyclic core and halogenated 6-membered rings. In effect, the HOMOs and LUMOs exhibited distinct spatial separation, affording multiple resonance structures that result in smaller effective band gaps. The computed HOMO–LUMO gaps were narrower than the estimated E_g^{opt} values: 1.85–1.87 vs 1.95–1.97 eV for F₈Bsub(PC₂-Nc₁)s, 1.77–1.81 vs 1.92–1.94 eV for (7a)–(7c), and 1.78–1.81 vs 1.87–1.89 eV for (9a)–(9c), but aligning consistently with previously described optical trends.

3. CONCLUSION

The lack of precision in macrocyclic chemistry is long-standing, particularly in mixed cyclotrimerizations for Bsub(PC_{3-p}-Nc_p) hybrids. To tackle this challenge, a new family of π -extended, bay-position phenylated R_a-Ph₂-(R_p)₈Bsub(PC₂-Nc₁) hybrids (R_a = Cl-, F-, or PhO-; R_p = Cl- or F-; $p = 1$) was precisely synthesized by sterically driven mixed cyclotrimerization. HPLC characterization unambiguously confirmed the controllable nature of this process guided by steric effects and carefully selected reaction conditions, achieving optimized selectivities (59% when R_p = Cl; 72% when R_p = F) and yields (29–59% when R_p = Cl; 19–39% when R_p = F) markedly higher than conventional methods. Computational studies on *ortho*-dinitrile precursors revealed the approach's sensitivity to Lewis basicity balances as an insight into hybrid macrocycle formation. Single-crystal analyses unveiled distinct packing motifs with the unused phenyl groups manifesting an oblique orientation to the macrocyclic scaffold. The R_a-Ph₂-(R_p)₈Bsub(PC₂-Nc₁) hybrids featured a bowl-shaped configuration accompanied by broad red-shifted absorption ($\text{fwhm}_{\text{sol}}^{\text{abs}} = 54.5\text{--}66.0\text{ nm}$, $\lambda_{\text{max, sol}}^{\text{abs}} = 621.5\text{--}643.0\text{ nm}$), sharp and narrow-band emission ($\text{fwhm}_{\text{sol}}^{\text{PL}} = 28.5\text{--}31.0\text{ nm}$), small band gap energies (<2.0 eV), and reversible electron-accepting capabilities. Harnessing site-specific steric hindrance, this study presents a synthetic route with minimized C_{3v}-macrocycle formation and increased selectivity toward tailored C_s-symmetric Bsub(PC₂-Nc₁) hybrids, advancing the development of bespoke macrocycles with unique optical and electronic properties. More importantly, controlled

synthetic strategies of this kind are anticipated to accelerate the exploration of ring-contracted porphyrinoid hybrids, customizing them for optimal performance in fine-tuned optoelectronic devices.

■ ASSOCIATED CONTENT

Data Availability Statement

CCDC deposition numbers 2305675–2305681 contain the supplementary crystallographic data for this paper. These data can be obtained free of charge via www.ccdc.cam.ac.uk/data_request/cif, or by emailing data_request@ccdc.cam.ac.uk, or by contacting The Cambridge Crystallographic DataCentre, 12 Union Road, Cambridge CB2 1EZ, UK; fax: + 441223 336033.

SI Supporting Information

The Supporting Information is available free of charge at <https://pubs.acs.org/doi/10.1021/prechem.4c00012>.

Equations, general experimental methods, detailed synthetic procedures, characterization data for new compounds, DFT calculation details, X-ray crystallographic data, and additional electrochemistry (PDF)

Crystallographic data for CCDC 2305675 (CIF)

Crystallographic data for CCDC 2305676 (CIF)

Crystallographic data for CCDC 2305677 (CIF)

Crystallographic data for CCDC 2305678 (CIF)

Crystallographic data for CCDC 2305679 (CIF)

Crystallographic data for CCDC 2305680 (CIF)

Crystallographic data of CCDC 2305681 (CIF)

SMILES data for all compounds investigated computationally in this publication (XLSX)

■ AUTHOR INFORMATION

Corresponding Author

Timothy P. Bender – Department of Chemical Engineering and Applied Chemistry, University of Toronto, Toronto, Ontario MSS 3E5, Canada; Department of Chemistry, University of Toronto, Toronto, Ontario MSS 3H6, Canada; Department of Materials Science and Engineering, University of Toronto, Toronto, Ontario MSS 3E4, Canada; Department of

Mechanical and Industrial Engineering, University of Toronto, Toronto, Ontario M5S 3G8, Canada; orcid.org/0000-0002-6086-7445; Email: tim.bender@utoronto.ca

Authors

Nina F. Farac – Department of Chemical Engineering and Applied Chemistry, University of Toronto, Toronto, Ontario M5S 3E5, Canada; orcid.org/0000-0002-8886-2187

Alan J. Lough – Department of Chemistry, University of Toronto, Toronto, Ontario M5S 3H6, Canada; orcid.org/0000-0001-6012-0379

Complete contact information is available at:

<https://pubs.acs.org/10.1021/prechem.4c00012>

Author Contributions

A.J.L. diffracted all single crystals and acquired all X-ray diffracted crystallographic data. N.F.F. conducted all chemical syntheses including separations and purifications, obtained full characterization (HPLC, NMR, MS, UV–vis absorption, photoluminescence, quantum yields, CV, DPV), grew single crystals for diffraction, carried out all DFT computations, analyzed all acquired data, and put the manuscript together. N.F.F. and T.P.B. developed the synthetic designs and contributed to revising and editing the manuscript. This project was completed under the supervision of T.P.B.

Notes

The authors declare no competing financial interest.

ACKNOWLEDGMENTS

The computational work was made possible by the facilities of the Shared Hierarchical Academic Research Computing Network (SHARCNET: www.sharcnet.ca) and Digital Research Alliance of Canada (www.alliancecan.ca/en). N.F.F. is grateful for a Postgraduate Scholarship (PGS D) at the University of Toronto (Canada) from the Natural Sciences and Engineering Research Council (NSERC) of Canada, a Hatch Graduate Scholarship from Hatch Ltd (Mississauga, Ontario, Canada), and for the support from Climate Positive Energy (CPE) at the University of Toronto (Canada). The authors also gratefully acknowledge the NSERC of Canada and their support of this work through a Discovery Grant (DG) to T.P.B.

REFERENCES

- (1) Grant, T. M.; Josey, D. S.; Sampson, K. L.; Mudigonda, T.; Bender, T. P.; Lessard, B. H. Boron Subphthalocyanines and Silicon Phthalocyanines for Use as Active Materials in Organic Photovoltaics. *Chem. Rec.* **2019**, *19* (6), 1093–1112.
- (2) Labella, J.; Torres, T. Subphthalocyanines: Contracted Porphyrinoids with Expanded Applications. *Trends Chem.* **2023**, *5* (5), 353–366.
- (3) Cnops, K.; Rand, B. P.; Cheyns, D.; Verreert, B.; Empl, M. A.; Heremans, P. 8.4% Efficient Fullerene-Free Organic Solar Cells Exploiting Long-Range Exciton Energy Transfer. *Nat. Commun.* **2014**, *5*, 3406.
- (4) Cnops, K.; Zango, G.; Genoe, J.; Heremans, P.; Martinez-Diaz, M. V.; Torres, T.; Cheyns, D. Energy Level Tuning of Non-Fullerene Acceptors in Organic Solar Cells. *J. Am. Chem. Soc.* **2015**, *137* (28), 8991–8997.
- (5) Verreert, B.; Cnops, K.; Cheyns, D.; Heremans, P.; Stesmans, A.; Zango, G.; Claessens, C. G.; Torres, T.; Rand, B. P. Decreased Recombination Through the Use of a Non-Fullerene Acceptor in a 6.4% Efficient Organic Planar Heterojunction Solar Cell. *Adv. Energy Mater.* **2014**, *4* (8), 1301413.
- (6) Ma, B.; Woo, C. H.; Miyamoto, Y.; Fréchet, J. M. J. Solution Processing of a Small Molecule, Subnaphthalocyanine, for Efficient Organic Photovoltaic Cells. *Chem. Mater.* **2009**, *21* (8), 1413–1417.
- (7) Endres, J.; Pelczar, L.; Rand, B. P.; Kahn, A. Determination of Energy Level Alignment within an Energy Cascade Organic Solar Cell. *Chem. Mater.* **2016**, *28* (3), 794–801.
- (8) Dang, J. D.; Josey, D. S.; Lough, A. J.; Li, Y.; Sifate, A.; Lu, Z.-H.; Bender, T. P. The Mixed Alloyed Chemical Composition of Chloro-(Chloro)n-Boron Subnaphthalocyanines Dictates their Physical Properties and Performance in Organic Photovoltaic Devices. *J. Mater. Chem. A* **2016**, *4* (24), 9566–9577.
- (9) Nikolis, V. C.; Benduhn, J.; Holzmüller, F.; Piersimoni, F.; Lau, M.; Zeika, O.; Neher, D.; Koerner, C.; Spoltore, D.; Vandewal, K. Reducing Voltage Losses in Cascade Organic Solar Cells while Maintaining High External Quantum Efficiencies. *Adv. Energy Mater.* **2017**, *7* (21), 1700855.
- (10) Labella, J.; Shoyama, K.; Guzmán, D.; Schembri, T.; Stolte, M.; Torres, T.; Würthner, F. Naphthalimide-Fused Subphthalocyanines: Electron-Deficient Materials Prepared by Cascade Annulation. *ACS Materials Lett.* **2023**, *5* (2), 543–548.
- (11) Álvaro-Martins, M. J.; Sánchez, J. G.; Lavarda, G.; Molina, D.; Pallarès, J.; Torres, T.; Marsal, L. F.; Sastre-Santos, A. Subphthalocyanine-Diketopyrrolopyrrole Conjugates: 3D Star-Shaped Systems as Non-Fullerene Acceptors in Polymer Solar Cells with High Open-Circuit Voltage. *ChemPlusChem.* **2021**, *86* (10), 1366–1373.
- (12) Plint, T. G.; Lessard, B. H.; Bender, T. P. Doping Chloro Boron Subnaphthalocyanines and Chloro Boron Subphthalocyanine in Simple OLED Architectures Yields Warm White Incandescent-like Emissions. *Opt. Mater.* **2018**, *75*, 710–718.
- (13) Josey, D. S.; Ingram, G. L.; Garner, R. K.; Wang, J. M.; Evans, G. J.; Lu, Z.-H.; Bender, T. P. Outdoor Stability of Chloro-(Chloro)n-Boron Subnaphthalocyanine and Chloro-Boron Subphthalocyanine as Electron Acceptors in Bilayer and Trilayer Organic Photovoltaics. *ACS Appl. Energy Mater.* **2019**, *2* (2), 979–986.
- (14) Josey, D. S.; Nyikos, S. R.; Garner, R. K.; Dovijarski, A.; Castrucci, J. S.; Wang, J. M.; Evans, G. J.; Bender, T. P. Outdoor Performance and Stability of Boron Subphthalocyanines Applied as Electron Acceptors in Fullerene-Free Organic Photovoltaics. *ACS Energy Lett.* **2017**, *2* (3), 726–732.
- (15) Bukuroshi, E.; Petersen, A. U.; Broløs, L.; Bender, T. P.; Nielsen, M. B. Exploring the Synthesis and Electronic Properties of Axially Substituted Boron Subphthalocyanines with Carbon-Based Functional Groups. *Eur. J. Inorg. Chem.* **2020**, *2020* (36), 3481–3495.
- (16) Dowds, M.; Nielsen, M. B. Controlling the Optical Properties of Boron Subphthalocyanines and Their Analogues. *Mol. Syst. Des. Eng.* **2021**, *6* (1), 6–24.
- (17) Labella, J.; Lavarda, G.; Hernández-López, L.; Aguilar-Galindo, F.; Díaz-Tendero, S.; Lobo-Checa, J.; Torres, T. Preparation, Supramolecular Organization, and On-Surface Reactivity of Enantio-pure Subphthalocyanines: From Bulk to 2D-Polymerization. *J. Am. Chem. Soc.* **2022**, *144* (36), 16579–16587.
- (18) Claessens, C. G.; Torres, T. Synthesis of Unsymmetrically Substituted Subphthalocyanines. *Chem.—Eur. J.* **2000**, *6* (12), 2168–2172.
- (19) González-Rodríguez, D.; Claessens, C. G.; Torres, T. Synthesis of Low-Symmetry Subphthalocyanines with Diverse Functionalization Patterns. *J. Porphy. Phthalocyanines* **2009**, *13* (2), 203–214.
- (20) Gotfredsen, H.; Storm, F. E.; Munoz, A. V.; Santella, M.; Kadziola, A.; Hammerich, O.; Mikkelsen, K. V.; Nielsen, M. B. Thieno-Fused Subporphyrazines: A New Class of Light Harvesters. *Chem.—Eur. J.* **2017**, *23* (64), 16194–16198.
- (21) Hamdoush, M.; Skvortsov, I. A.; Mikhailov, M. S.; Pakhomov, G.; Stuzhin, P. A. Perfluorinated Subphthalocyanine Analogues Containing Fused 1,2,5-Thiadiazole Fragments. *J. Fluor. Chem.* **2017**, *204*, 31–36.
- (22) Pakhomov, G. L.; Travkin, V. V.; Hamdoush, M.; Zhabanov, Y. A.; Stuzhin, P. A. Thiadiazole Fused Subporphyrazines as Acceptors in Organic Photovoltaic Cells. *Macroheterocycles* **2017**, *10* (4–5), 548–551.

- (23) Wang, Y.; Mori, S.; Furuta, H.; Shimizu, S. Bis(1,3-dithiol-2-ylidene)-Substituted Subtriazachlorin: a Subphthalocyanine Analogue with Redox Properties. *Angew. Chem., Int. Ed.* **2019**, *58*, 10975–10979.
- (24) Ince, M.; Medina, A.; Yum, J. H.; Yella, A.; Claessens, C. G.; Martinez-Diaz, M. V.; Gratzel, M.; Nazeeruddin, M. K.; Torres, T. Peripherally and Axially Carboxylic Acid Substituted Subphthalocyanines for Dye-Sensitized Solar Cells. *Chem.—Eur. J.* **2014**, *20* (7), 2016–2021.
- (25) Urbani, M.; Sari, F. A.; Gratzel, M.; Nazeeruddin, M. K.; Torres, T.; Ince, M. Effect of Peripheral Substitution on the Performance of Subphthalocyanines in DSSCs. *Chem.—Asian J.* **2016**, *11* (8), 1223–1231.
- (26) Zango, G.; Sakurai, T.; Urones, B.; Saeki, H.; Matsuda, W.; Martinez-Diaz, M. V.; Seki, S.; Torres, T. Peripherally Cyanated Subphthalocyanines as Potential n-Type Organic Semiconductors. *Chem.—Eur. J.* **2018**, *24* (33), 8331–8342.
- (27) Zango, G.; Zirzmeier, J.; Claessens, C. G.; Clark, T.; Martinez-Diaz, M. V.; Guldi, D. M.; Torres, T. A Push-Pull Unsymmetrical Subphthalocyanine Dimer. *Chem. Sci.* **2015**, *6* (10), 5571–5577.
- (28) Skvortsov, I. A.; Chufarin, A. E.; Zaitsev, M. V.; Kirakosyan, G. A.; Stuzhin, P. A. First Subphthalocyanine Analogue with Fused 6H-1,4-diazepine Ring and its Conversion to Aminobenzamide Derivative. *Asian J. Org. Chem.* **2023**, *12* (11), No. e202300425.
- (29) Li, Z.; Gong, Q.; Hao, E.; Jiao, L. B(III)-subporphyrines, B(III)-subporphyrins and their hybrids. *Coord. Chem. Rev.* **2023**, *493*, 215325.
- (30) Gottfredsen, H.; Neumann, T.; Storm, F. E.; Muñoz, A. V.; Jevric, M.; Hammerich, O.; Mikkelsen, K. V.; Freitag, M.; Boschloo, G.; Nielsen, M. B. Donor-Acceptor-Functionalized Subphthalocyanines for Dye-Sensitized Solar Cells. *ChemPhotoChem.* **2018**, *2* (11), 976–985.
- (31) Kamino, B. A.; Bender, T. P. Modified Boron Subphthalocyanines with Stable Electrochemistry and Tuneable Bandgaps. *Dalton Trans.* **2013**, *42* (36), 13145–13150.
- (32) Shimizu, S.; Nakano, S.; Hosoya, T.; Kobayashi, N. Pyrene-Fused Subphthalocyanine. *Chem. Commun.* **2011**, *47* (1), 316–318.
- (33) Shimizu, S.; Furuta, H. Core-Modified Phthalocyanines and Subphthalocyanines: a Synthetic Strategy towards Core-Modification and Novel Properties Arising from the Inner Ring-Expansion. *Macromolecules* **2015**, *48* (4), 332–342.
- (34) Shimizu, S.; Kobayashi, N. Structurally-Modified Subphthalocyanines: Molecular Design Towards Realization of Expected Properties From the Electronic Structure and Structural Features of Subphthalocyanine. *Chem. Commun.* **2014**, *50* (53), 6949–6966.
- (35) Shimizu, S.; Nakano, S.; Kojima, A.; Kobayashi, N. A Core-Expanded Subphthalocyanine Analogue with a Significantly Distorted Conjugated Surface and Unprecedented Properties. *Angew. Chem., Int. Ed.* **2014**, *53* (9), 2408–2412.
- (36) Farac, N. F.; Tetreault, A. R.; Bender, T. P. Cs-Symmetric, Peripherally Fluorinated Boron Subphthalocyanine-Subnaphthalocyanine Hybrids: Shedding New Light on Their Fundamental Photo-physical Properties and Their Functionality as Optoelectronic Materials. *J. Phys. Chem. C* **2023**, *127* (1), 702–727.
- (37) Mack, J.; Otaki, T.; Durfee, W. S.; Kobayashi, N.; Stillman, M. J. MCD Spectroscopy and TD-DFT Calculations of Low Symmetry Subnaphthalocyanine Analogs. *J. Inorg. Biochem.* **2014**, *136*, 122–129.
- (38) McAuliffe, K. J.; Kaster, M. A.; Szig, R. G.; Trivedi, E. R. Low-Symmetry Mixed Fluorinated Subphthalocyanines as Fluorescence Imaging Probes in MDA-MB-231 Breast Tumor Cells. *Int. J. Mol. Sci.* **2017**, *18*, 1177.
- (39) Stork, J. R.; Potucek, R. J.; Durfee, W. S.; Noll, B. C. The Synthesis and Structure of Mixed Subphthalocyanine/Subnaphthalocyanine Complexes. *Tetrahedron Lett.* **1999**, *40*, 8055–8058.
- (40) Zyskowski, C. D.; Kennedy, V. O. Compounds in the Series from Boron Subphthalocyanine to Boron Subnaphthalocyanine. *J. Porphyr. Phthalocyanines* **2000**, *4*, 707–712.
- (41) Lavarda, G.; Labella, J.; Martínez-Díaz, M. V.; Rodríguez-Morgade, M. S.; Osuka, A.; Torres, T. Recent Advances in Subphthalocyanines and Related Subporphyrinoids. *Chem. Soc. Rev.* **2022**, *51* (23), 9482–9619.
- (42) Li, Z.; Zhang, L.; Wu, Q.; Li, H.; Kang, Z.; Yu, C.; Hao, E.; Jiao, L. Boron-Templated Synthesis of B(III)-Submonoazaporphyrins: The Hybrids of B(III)-Subporphyrins and B(III)-Subporphyrazines. *J. Am. Chem. Soc.* **2022**, *144* (15), 6692–6697.
- (43) Remiro-Buenamañana, S.; Díaz-Moscoso, A.; Hughes, D. L.; Bochmann, M.; Tizzard, G. J.; Coles, S. J.; Cammidge, A. N. Synthesis of Meso-Substituted Subphthalocyanine-Subporphyrin Hybrids: Boron Subtribenzodiazaporphyrins. *Angew. Chem., Int. Ed.* **2015**, *54* (26), 7510–7514.
- (44) Tejerina, L.; Martínez-Díaz, M. V.; Torres, T. One-Pot Synthesis of π -Extended Fluorenone-Fused Subphthalocyanines. *Org. Lett.* **2019**, *21* (8), 2908–2912.
- (45) Nemykin, V. N.; Dudkin, S. V.; Dumoulin, F.; Hirel, C.; Gürek, A. G.; Ahsen, V. Synthetic Approaches to Asymmetric Phthalocyanines and Their Analogues. *ARKIVOC* **2014**, *2014* (1), 142–204.
- (46) Chan, J. Y. M.; Ng, D. K. P. [3 + 1] Mixed Cyclization: A Synthetic Route to Prepare Low-Symmetry Phthalocyanines. *J. Org. Chem.* **2022**, *87* (11), 7213–7218.
- (47) Chow, S. Y. S.; Ng, D. K. P. Synthesis of an ABCD-Type Phthalocyanine by Intramolecular Cyclization Reaction. *Org. Lett.* **2016**, *18* (13), 3234–3237.
- (48) Sejdarasi, L.; McAuliffe, K. J.; Corbin, B. A.; Trivedi, E. R. Synthesis and Characterization of Mixed Fluorinated Phenylthio-Subphthalocyanines. *ChemistrySelect* **2017**, *2* (24), 7417–7420.
- (49) Kudo, R.; Kitamura, K.; Hamura, T. 1,3-Dialkynyl- and 1,3-Dialkenylisobenzofurans: New π -Extended Congeners Prepared by Double Nucleophilic Addition of Alkynyllithiums to o-Phthalaldehyde. *Chem. Lett.* **2017**, *46* (1), 25–28.
- (50) Benderradj, F.; Nechab, M.; Einhorn, C.; Einhorn, J. A Single-Step Synthesis of Symmetrical 1,3-Diarylisobenzofurans. *Synlett* **2006**, *2006* (13), 2035–2038.
- (51) de Souza, T. F. M.; Torres Antonio, F. C.; Homem-de-Mello, P.; Ribeiro, A. O. Unsymmetrical Zinc (II) Phthalocyanine and Zinc (II) Naphthalocyanine with 2,3-Dicyano-1,4-Diphenyl-naphthalene Precursor. *Dyes Pigm.* **2020**, *172*, 107824.
- (52) Hildebrand, M.; Holst, D.; Bender, T.; Kronik, L. Electronic Structure, Bonding, and Stability of Boron Subphthalocyanine Halides and Pseudohalides. *Adv. Theory Simul.* **2022**, *5* (4), 2100400.
- (53) Fulford, M. V.; Jaidka, D.; Paton, A. S.; Morse, G. E.; Brisson, E. R. L.; Lough, A. J.; Bender, T. P. Crystal Structures, Reaction Rates, and Selected Physical Properties of Halo-Boron-subphthalocyanines (Halo = Fluoride, Chloride, and Bromide). *J. Chem. Eng. Data* **2012**, *57* (10), 2756–2765.
- (54) Ilyas, N.; Hariviyasi, S. S.; Zahl, P.; Cortes, R.; Hofmann, O. T.; Sutter, P.; Zojer, E.; Monti, O. L. A. Sticking with the Pointy End? Molecular Configuration of Chloro Boron-Subphthalocyanine on Cu(111). *J. Phys. Chem. C* **2016**, *120* (13), 7113–7121.
- (55) Guilleme, J.; Martínez-Fernández, L.; González-Rodríguez, D.; Corral, I.; Yáñez, M.; Torres, T. An Insight into the Mechanism of the Axial Ligand Exchange Reaction in Boron Subphthalocyanine Macrocycles. *J. Am. Chem. Soc.* **2014**, *136* (40), 14289–14298.
- (56) Bukuroshi, E.; Vestfrid, J.; Gross, Z.; Bender, T. P. Fluorinated Boron Subphthalocyanines: Lewis Acid Based Templating Chemistry Facilitates Random Halide Exchange, and Fluoride versus Chloride Affects the Basic Photophysical Properties and the Solid-State Arrangement. *New J. Chem.* **2019**, *43* (42), 16730–16737.
- (57) Guilleme, J.; González-Rodríguez, D.; Torres, T. Triflate-Subphthalocyanines: Versatile, Reactive Intermediates for Axial Functionalization at the Boron Atom. *Angew. Chem., Int. Ed.* **2011**, *50* (15), 3506–3509.
- (58) Paton, A. S.; Lough, A. J.; Bender, T. P. A Role for π -Br Interactions in the Solid-State Molecular Packing of Para-Halo-Phenoxy-Boron-subphthalocyanines. *CrystEngComm* **2011**, *13* (11), 3653–3656.
- (59) Dang, J. D.; Josey, D. S.; Dang, M. T.; Bender, T. P. Phenoxy-(Chloro)n-Boron Subnaphthalocyanines: Alloyed Mixture, Electron-Accepting Functionality, and Enhanced Solubility for Bulk Heterojunction Organic Photovoltaics. *ACS Omega* **2018**, *3* (2), 2093–2103.

(60) González-Rodríguez, D.; Torres, T.; Guldi, D. M.; Rivera, J.; Herranz, M. Á.; Echegoyen, L. Subphthalocyanines: Tuneable Molecular Scaffolds for Intramolecular Electron and Energy Transfer Processes. *J. Am. Chem. Soc.* **2004**, *126* (20), 6301–6313.

(61) Sampson, K. L.; Jiang, X.; Bukuroshi, E.; Dovijarski, A.; Raboui, H.; Bender, T. P.; Kadish, K. M. A Comprehensive Scope of Peripheral and Axial Substituent Effect on the Spectroelectrochemistry of Boron Subphthalocyanines. *J. Phys. Chem. A* **2018**, *122* (18), 4414–4424.

(62) Holst, D. P.; Dovijarski, A.; Lough, A. J.; Bender, T. P. Triphenyl Borates Used to Avoid the Bay-Position Halogenation of Boron Subnaphthalocyanines; and for the Subnaphthalocyanine, Subphthalocyanine and Hybrids Formation. *New J. Chem.* **2024**, *48*, 5127.

(63) Laurence, C.; Graton, J.; Gal, J.-F. An Overview of Lewis Basicity and Affinity Scales. *J. Chem. Educ.* **2011**, *88* (12), 1651–1657.

(64) Legault, C. Y. *CYView*, 1.0b; Université de Sherbrooke, 2009. <https://www.cylview.org/>.

(65) Claessens, C. G.; González-Rodríguez, D.; Rodríguez-Morgade, M. S.; Medina, A.; Torres, T. Subphthalocyanines, Subporphyrines, and Subporphyrins: Singular Nonplanar Aromatic Systems. *Chem. Rev.* **2014**, *114* (4), 2192–2277.

(66) Morse, G. E.; Gong, I.; Kawar, Y.; Lough, A. J.; Bender, T. P. Crystal and Solid-State Arrangement Trends of Halogenated Boron Subphthalocyanines. *Cryst. Growth Des.* **2014**, *14* (5), 2138–2147.

(67) Virdo, J. D.; Lough, A. J.; Bender, T. P. Redetermination of the Crystal Structure of Boron Subphthalocyanine Chloride (Cl-BsubPc) Enabled by Slow Train Sublimation. *Acta Crystallogr., Sect. C: Struct. Chem.* **2016**, *72* (4), 297–307.

(68) Wojtkiewicz, K.; Lough, A.; Bender, T. P. Analysis of the Solvent Effects on the Crystal Growth of Peripherally Chlorinated Boron Subphthalocyanines. *CrystEngComm* **2022**, *24* (15), 2791–2807.

(69) Wróbel, D.; Siejak, A.; Siejak, P. Photovoltaic and Spectroscopic Studies of Selected Halogenated Porphyrins for Their Application in Organic Solar Cells. *Sol. Energy Mater. Sol. Cells* **2010**, *94* (3), 492–500.

(70) Sampson, K. L.; Josey, D. S.; Li, Y.; Virdo, J. D.; Lu, Z.-H.; Bender, T. P. Ability To Fine-Tune the Electronic Properties and Open-Circuit Voltage of Phenoxy-Boron Subphthalocyanines through Meta-Fluorination of the Axial Substituent. *J. Phys. Chem. C* **2018**, *122* (2), 1091–1102.

(71) Williams, A. T. R.; Winfield, S. A.; Miller, J. N. Relative Fluorescence Quantum Yields Using a Computer-Controlled Luminescence Spectrometer. *Analyst* **1983**, *108* (1290), 1067–1071.

(72) Ghodbane, A.; Saffon, N.; Blanc, S.; Fery-Forgues, S. Influence of the Halogen Atom on the Solid-State Fluorescence Properties of 2-Phenyl-Benzoxazole Derivatives. *Dyes Pigm.* **2015**, *113*, 219–226.

(73) Xiang, Y.; Zhao, Y.; Xu, N.; Gong, S.; Ni, F.; Wu, K.; Luo, J.; Xie, G.; Lu, Z.-H.; Yang, C. Halogen-Induced Internal Heavy-Atom Effect Shortening the Emissive Lifetime and Improving the Fluorescence Efficiency of Thermally Activated Delayed Fluorescence Emitters. *J. Mater. Chem. C* **2017**, *5* (46), 12204–12210.

(74) Bukuroshi, E.; Wong, S.; Mudigonda, T.; Nova, K.; Dumont, A.; Holst, D.; Lu, Z.-H.; Bender, T. P. Molecular Engineering of α and β Peripherally Tri-Halogenated Substituted Boron Subphthalocyanines as Mixed Alloys to Control Physical and Electrochemical Properties for Organic Photovoltaic Applications. *Mol. Syst. Des. Eng.* **2021**, *6* (4), 308–326.

(75) Mizrahi, A.; Bukuroshi, E.; Vestfrid, J.; Bender, T. P.; Gross, Z. Axial/Peripheral Chloride/Fluoride-Substituted Boron Subphthalocyanines as Electron Acceptors. *Inorg. Chem.* **2020**, *59* (5), 2641–2645.

(76) D'Andrade, B. W.; Datta, S.; Forrest, S. R.; Djurovich, P.; Polikarpov, E.; Thompson, M. E. Relationship Between the Ionization and Oxidation Potentials of Molecular Organic Semiconductors. *Org. Electron.* **2005**, *6* (1), 11–20.

(77) Holst, D. P.; Friederich, P.; Aspuru-Guzik, A.; Bender, T. P. Updated Calibrated Model for the Prediction of Molecular Frontier Orbital Energies and Its Application to Boron Subphthalocyanines. *J. Chem. Inf. Model.* **2022**, *62* (4), 829–840.